Inorg. Chem. **2003**, *42*, 4680–4695

Connecting Terminal Carboxylate Groups in Nine-Coordinate Lanthanide Podates: Consequences on the Thermodynamic, Structural, Electronic, and Photophysical Properties

Jean-Michel Senegas,[†] Gérald Bernardinelli,[‡] Daniel Imbert,[§] Jean-Claude G. Bünzli,[§] Pierre-Yves Morgantini,[||] Jacques Weber,[||] and Claude Piguet*[,†]

Department of Inorganic, Analytical and Applied Chemistry and Department of Physical Chemistry, University of Geneva, 30 quai E. Ansermet, CH-1211 Geneva 4, Switzerland, Laboratory of X-ray Crystallography, University of Geneva, 24 quai E. Ansermet, CH-1211 Geneva 4, Switzerland, and Institute of Molecular and Biological Chemistry, Swiss Federal Institute of Technology, BCH 1402, CH-1015 Lausanne, Switzerland

Received March 3, 2003

The hydrolysis of terminal ^{t}butyl-ester groups provides the novel nonadentate podand tris{2-[*N*-methylcarbamoyl-(6-carboxypyridine-2)-ethyl]amine} (L13) which exists as a mixture of slowly interconverting conformers in solution. At pH = 8.0 in water, its deprotonated form $[L13 - 3H]^{3-}$ reacts with $Ln(ClO_4)_3$ to give the poorly soluble and stable podates [Ln(L13 − 3H)] ($\log(\beta_{110}) = 6.7–7.0$, Ln = La–Lu). The isolated complexes $[Ln(L13 - 3H)](H_2O)_7$ (Ln = Eu, **8**; Tb, **9**; Lu, **10**) are isostructural, and their crystal structures show Ln(III) to be nine-coordinate in a pseudotricapped trigonal prismatic site defined by the donor atoms of the three helically wrapped tridentate binding units of L13. The Ln–O(carboxamide) bonds are only marginally longer than the Ln–O(carboxylate) bonds in [Ln(L13 − 3H)], thus producing a regular triple helix around Ln(III) which reverses its screw direction within the covalent Me–TREN tripod. High-resolution emission spectroscopy demonstrates that (i) the replacement of terminal carboxamides with carboxylates induces only minor electronic changes for the metallic site, (ii) the solid-state structure is maintained in water, and (iii) the metal in the podate is efficiently protected from interactions with solvent molecules. The absolute quantum yields obtained for [Eu(L13 − 3H)] ($\Phi_{Eu}^{tot} = 1.8 \times 10^{-3}$) and [Tb(L13 − 3H)] ($\Phi_{Eu}^{tot} = 8.9 \times 10^{-3}$) in water remain modest and strongly contrast with that obtained for the lanthanide luminescence step ($\Phi^{Eu} = 0.28$). Detailed photophysical studies assign this discrepancy to the small energy gap between the ligand-centered singlet ($^1\pi\pi^*$) and triplet ($^3\pi\pi^*$) states which limits the efficiency of the intersystem crossing process. Theoretical TDDFT calculations suggest that the connection of a carboxylate group to the central pyridine ring prevents the sizable stabilization of the triplet state required for an efficient sensitization process. The thermodynamic and electronic origins of the advantages (stability, lanthanide quantum yield) and drawbacks (solubility, sensitization) brought by the "carboxylate effect" in lanthanide complexes are evaluated for programming predetermined properties in functional devices.

Introduction

Although the close correlations between weak crystal-field effects and electronic[1] and magnetic[2] properties in lanthanide complexes were recognized early, it is only recently that multidentate ligands have been designed for programming specific coordination sites capable of inducing predetermined functions in molecular lanthanide-containing edifices.[3] Owing to the poor stereochemical preferences of Ln(III) and to the tendency of these species to adopt large and variable coordination numbers,[3,4] semirigid tridentate aromatic chelating units such as L1−L5 have attracted considerable interest because the wrapping of the ligand strands in the final D_3 symmetrical complexes $[Ln(L1 - 2H)_3]^{3-}$ and $[Ln(Li)_3]^{3+}$ ($i = 2-5$) provides well-defined nine-coordinate pseudo-

* Corresponding author. E-mail: Claude.Piguet@chiam.unige.ch.
[†] Department of Inorganic Chemistry, University of Geneva.
[‡] Laboratory of X-ray Crystallography, University of Geneva.
[§] Institute of Molecular and Biological Chemistry, Swiss Federal Institute of Technology.
[||] Department of Physical Chemistry, University of Geneva.

10.1021/ic034231t CCC: $25.00
Published on Web 06/20/2003

Chart 1

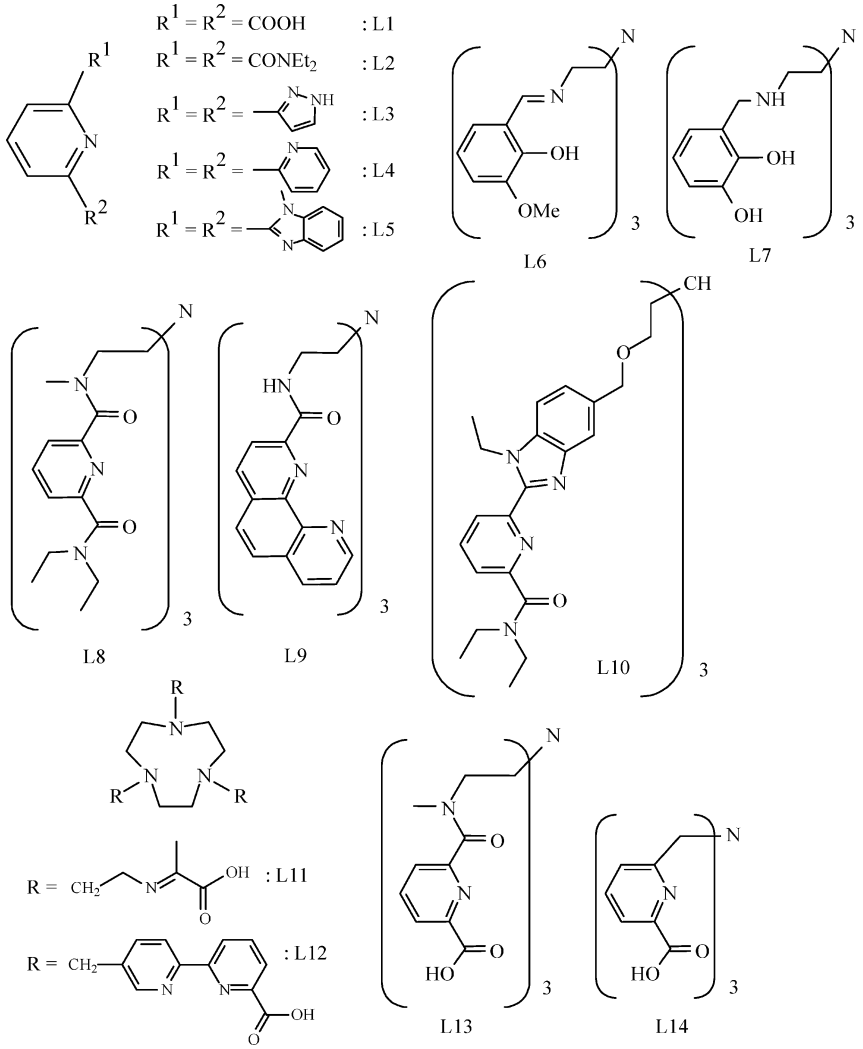

tricapped trigonal prismatic lanthanide sites.[5] Improved structural control and electronic tuning result from the use of unsymmetrical tridentate binding units ($R^1 \neq R^2$, Chart 1),[6] and various relevant aromatic-containing chelating units have been connected to covalent tripods in the nonadentate podands L6,[7] L7,[8] L8,[9] L9,[10] L10,[11] L11,[12] and L12[13] which

(1) For reviews see: (a) Carnall, W. T. In *Handbook on the Physics and Chemistry of Rare Earths*; Gschneidner, K. A., Jr., Eyring L., Eds.; North-Holland Publishing Company: Amsterdam, 1979; pp 171−208. (b) Görller-Walrand, C.; Binnemans, K. In *Handbook on the Physics and Chemistry of Rare Earths*; Gschneidner, K. A., Jr., Eyring L., Eds.; North-Holland Publishing Company: Amsterdam, 1996; Vol. 23, pp 121−283. (c) Porcher, P. In *Rare Earths*; Saez Puche, R., Caro, P., Eds.; Editorial Complutense S. A.: Madrid, 1998; pp 43−66. (d) Görller-Walrand, C.; Binnemans, K. In *Handbook on the Physics and Chemistry of Rare Earths*; Gschneidner, K. A., Jr., Eyring L., Eds.; North-Holland Publishing Company: Amsterdam, 1998; Vol. 25, pp 101−264.

(2) (a) Abragam, A.; Bleaney, B. *Electron Paramagnetic Resonance of Transitions Ions*; Clarendon Press: Oxford, 1970. (b) Mironov, V. S.; Galyametdinov, Y. G.; Ceulemans, A.; Görller-Walrand, C.; Binnemans, K. *J. Chem. Phys.* **2002**, *116*, 4673. (c) Ishikawa, N.; Iino, T.; Kaizu, Y. *J. Phys. Chem. A.* **2002**, *106*, 9543.

(3) (a) Parker, D.; Dickins, R. S.; Puschmann, H.; Crossland, C.; Howard, J. A. K. *Chem. Rev.* **2002**, *102*, 1977. (b) Bünzli, J.-C. G.; Piguet, C. *Chem. Rev.* **2002**, *102*, 1897. (c) Karmazin, L.; Mazzanti, M.; Gateau, C.; Hill, C.; Pécaut, J. *Chem. Commun.* **2002**, 2892.

(4) (a) Choppin, G. R. In *Lanthanide Probes in Life, Chemical and Earth Sciences*; Bünzli, J.-C. G., Choppin, G. R., Eds.; Elsevier: Amsterdam, 1989; Chapter 1, pp 1−41. (b) Bünzli, J.-C. G.; Milicic-Tang, A. In *Handbook on the Physics and Chemistry of Rare Earths*; Gschneidner, K. A., Jr., Eyring L., Eds.; Elsevier: Amsterdam, 1995; Vol. 21, Chapter 145, p 305. (c) Bünzli, J.-C. G. In *Rare Earths*; Saez Puche, R., Caro, P., Eds.; Editorial Complutense S. A.: Madrid, 1998; pp 223−259.

(5) (a) Renaud, F.; Piguet, C.; Bernardinelli, G.; Bünzli, J.-C. G.; Hopfgartner, G. *Chem. Eur. J.* **1997**, *3*, 1646. (b) Bardwell, D. A.; Jeffery, J. C.; Jones, P. L.; McCleverty, J. A.; Psillakis, E.; Reeves, Z.; Ward, M. D. *J. Chem. Soc., Dalton Trans.* **1997**, 2079. (c) Petoud, S.; Bünzli, J.-C. G.; Renaud, F.; Piguet, C.; Schenk, K. J.; Hopfgartner, G. *Inorg. Chem.* **1997**, *36*, 5750. (d) Mürner, H.-R.; Chassat, E.; Thummel, R. P.; Bünzli, J.-C. G. *J. Chem. Soc., Dalton Trans.* **2000**, 2809. (e) Semenova, L. I.; Sobolev, A. N.; Skelton, B. W.; White, A. H. *Aust. J. Chem.* **1999**, *52*, 519. (f) Ouali, N.; Bocquet, B.; Rigault, S.; Morgantini, P.-Y.; Weber, J.; Piguet, C. *Inorg. Chem.* **2002**, *41*, 1436.

(6) Piguet, C.; Edder, C.; Rigault, S.; Bernardinelli, G.; Bünzli, J.-C. G.; Hopfgartner, G. *J. Chem. Soc., Dalton Trans.* **2000**, 3999.

(7) (a) Costes, J.-P.; Dupuis, A.; Commenges, G.; Lagrave, S.; Laurent, J.-P. *Inorg. Chim. Acta* **1999**, *285*, 49. (b) Costes, J.-P.; Nicodème, F. *Chem. Eur. J.* **2002**, *8*, 3442.

(8) Bismondo, A.; Di Bernardo, P.; Portanova, R.; Tolazzi, M.; Zanonato, P. L. *Polyhedron* **2002**, *21*, 1393.

(9) Renaud, F.; Piguet, C.; Bernardinelli, G.; Bünzli, J.-C. G.; Hopfgartner, G. *J. Am. Chem. Soc.* **1999**, *121*, 9326.

(10) Bretonnière, Y.; Wietzke, R.; Lebrun, C.; Mazzanti, M.; Pécaut, J. *Inorg. Chem.* **2000**, *39*, 3499.

(11) Koeller, S.; Bernardinelli G.; Bocquet, B.; Piguet, C. *Chem. Eur. J.* **2003**, *9*, 1062.

(12) Tei, L.; Baum, G.; Blake, A. J.; Fenske, D.; Schröder, M. *J. Chem. Soc., Dalton Trans.* **2000**, 2793.

react with Ln(III) to give the C_3 symmetrical podates [Ln(Li − 3H)] (i = 6, 7, 11, 12) and [Ln(Li)]$^{3+}$ (i = 8−10). For L6 and L7, the unfavorable formation of six-membered chelate rings with Ln(III) ions[14] produces unsaturated seven-[7] and six-coordinate[8] podates in which each strand is only bidentate. For L8−L10, the final nine-coordinate podates [Ln(Li)]$^{3+}$ display the expected pseudotricapped trigonal prismatic metallic site resulting from the helical wrapping of the three tridentate binding units. However, their existence is limited to poorly competing solvents (log(β_{11}) = 6.5−8.5 in anhydrous CH_3CN)[9−11] and the sensitization of the visible metal-centered luminescence for the Eu- and Tb-complexes remains modest despite the absence of solvent molecules in the first coordination sphere (absolute quantum yields in the range $1.1 \times 10^{-4} < \Phi_{Ln}^{tot} < 4.8 \times 10^{-3}$).[9,11] Anionic carboxylates in [Ln(Li − 3H)] (i = 11, 12) generate large thermodynamic stability,[12,13] resistance toward hydrolysis,[12,13] and sizable emission quantum yields.[13] Similar effects have been previously noticed in f−f bimetallic triple-stranded helicates,[15] and these are tentatively assigned to the increased rigidity of the Ln(III) coordination sphere provided by the strong electrostatic Ln−carboxylate bonds. The impressive gains in stability and in quantum yield observed when going from [Eu(L2)$_3$]$^{3+}$ ($\Phi_{Eu}^{tot} = 8.7 \times 10^{-5}$ in acetonitrile)[5a] to [Eu(L1 − 2H)$_3$]$^{3-}$ ($\Phi_{Eu}^{tot} = 1.9 \times 10^{-2}$ in water),[16] or from [Eu(L10)]$^{3+}$ ($\Phi_{Eu}^{tot} = 4.3 \times 10^{-3}$ in acetonitrile)[11] to [Eu(L12 − 2H)]$^{+}$ ($\Phi_{Eu}^{tot} = 0.12$ in water),[13] follow this trend and suggest that the use of terminal carboxylate groups is particularly attractive for producing water-stable luminescent probes. However, the debatable effects observed for the analogous Tb complexes when going from [Tb(L2)$_3$]$^{3+}$ ($\Phi_{Tb}^{tot} = 3.5 \times 10^{-2}$ in acetonitrile)[5a] to [Tb(L1 − 2H)$_3$]$^{3-}$ ($\Phi_{Tb}^{tot} = 1.4 \times 10^{-2}$ in water),[17] or from [Tb(L10)]$^{3+}$ ($\Phi_{Tb}^{tot} = 1.4 \times 10^{-3}$ in acetonitrile)[11] to [Tb(L12 − 2H)]$^{+}$ ($\Phi_{Tb}^{tot} = 0.10$ in water)[13] indicate that the replacement of carboxamides with carboxylates affects the electronic properties of the ligand-centered excited states responsible for the sensitization processes in Eu- and Tb-complexes.[18] To address the origins of the beneficial thermodynamic and electronic contributions brought by carboxylate groups in lanthanide complexes, we report here on the synthesis of the novel rigid podates [Ln(L13 − 3H)] which are identical to the parent complexes [Ln(L8)]$^{3+}$,[9] except for the hydrolysis of the terminal carboxamide groups. Particular attention has been focused on the structural, thermodynamic, and electronic changes which can be unambiguously attributed to the introduction of carboxylate donors and on their consequences for programming predetermined properties in lanthanide complexes.

Scheme 1 [a]

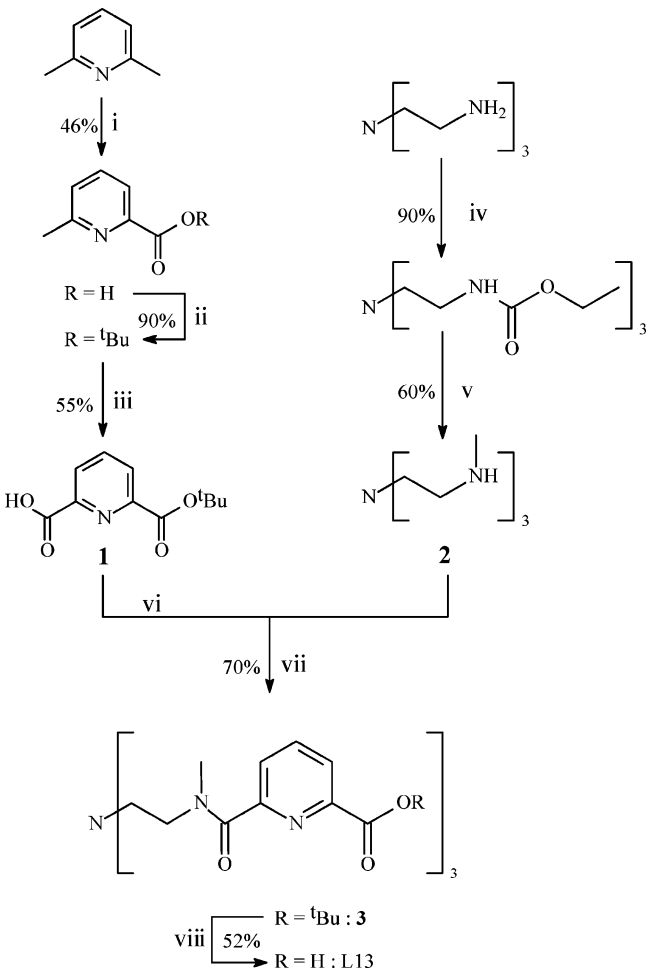

[a] Reagents: (i) $KMnO_4$, H_2O; (ii) (1) $SOCl_2$, CH_2Cl_2, $DMF_{cat.}$; (2) ^{t}BuOLi; (iii) SeO_2, pyridine; (iv) $ClCO_2Et$, KOH, C_6H_6−H_2O; (v) $LiAlH_4$, THF; (vi) $SOCl_2$, CH_2Cl_2, $DMF_{cat.}$; (vii) (^{i}prop)$_2$(Et)N, CH_2Cl_2; (viii) CF_3CO_2H.

Results and Discussion

Synthesis and Solution Structure of the Nonadentate Podand L13. Compared to the original synthetic strategy developed for the preparation of L8,[9] the introduction of terminal carboxylates in L13 requires their protection as ester groups which must be resistant toward acylation and coupling with tris((2-*N*-methylamino)ethyl)amine (Me−TREN, **2**), but reactive enough to allow their quantitative cleavage during the ultimate hydrolysis. Preliminary attempts using methyl- or benzylesters provided podands analogous to **3** which cannot be efficiently transformed into L13. The tert-butyl ester groups eventually fit our synthetic requirements, and reaction of Me−TREN (**2**)[19] with an excess of the acyl chloride derivative of the tridentate synthon **1** produces the podand **3** in fair yield (70%). Subsequent hydrolysis under smooth acidic conditions gives the hydrated podand L13·3H_2O (yield = 52%, Scheme 1). As a result of hindered rotations at room temperature about the OC−N bonds for

(13) Charbonnière, L. J.; Ziessel, R.; Guardigli, M.; Roda, A.; Sabbatini, N.; Cesario, M. *J. Am. Chem. Soc.* **2001**, *123*, 2436.
(14) Motekaitis, R. J.; Martell, A. E.; Hancock, R. A. *Coord. Chem. Rev.* **1994**, *133*, 39.
(15) (a) Elhabiri, M.; Scopelliti, R.; Bünzli, J.-C. G.; Piguet, C. *J. Am. Chem. Soc.* **1999**, *121*, 10747. (b) Lessmann, J. L.; Horrocks, W. DeW., Jr. *Inorg. Chem.* **2000**, *39*, 3114.
(16) (a) Richardson, F. S.; Metcalf, D. H.; Glover, D. P. *J. Phys. Chem.* **1991**, *95*, 6249. (b) An, Y.; Berry, M. T.; van Veggel, F. C. J. M. *J. Phys. Chem. A* **2000**, *104*, 11243.
(17) Renaud, F.; Piguet, C. Unpublished results.
(18) (a) Sabbatini, N.; Guardigli, M.; Lehn, J.-M. *Coord. Chem. Rev.* **1993**, *123*, 201. (b) Sabbatini, N.; Guardigli, M.; Manet, I. In *Handbook on the Physics and Chemistry of Rare Earths*; Gschneidner, K. A., Jr., Eyring L., Eds.; Elsevier: Amsterdam, 1996; Vol. 23, p 69−119.
(19) Schmidt, H.; Lensink, C.; Xi, S. K.; Verkade, J. G. *Z. Anorg. Allg. Chem.* **1989**, *578*, 75.

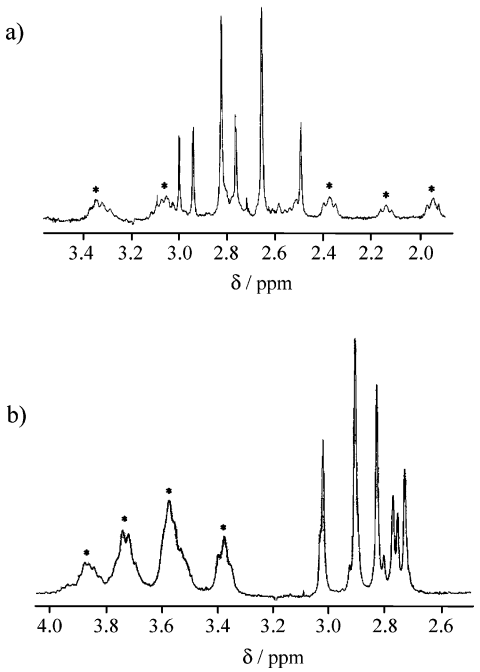

Figure 1. Part of the 300 MHz ^{1}H NMR spectra of (a) $[L13 - 3H]^{3-}$ (D_2O, pD = 10, 298K)[20] and (b) $[L13 - 2H]^{2-}$ (D_2O, pD = 5.2, 298 K)[20] showing the signals of the methyl protons (singlets) and of the ethylene spacers (*).

the three unsymmetrical tertiary amide connectors, L13 exists in solution as a mixture of conformers which are inert on the NMR time scale.[9] According to the *E* or *Z* arrangement of the ethylene spacer with respect to the oxygen atom of the amide group within each strand (i.e., the OC−N bond is considered as a double bond), a total of eight possible combinations provides four conformers in a 1:3:3:1 statistical ratio: *EEE* (C_{3v}, 12.5%), *EEZ* (C_s, 37.5%), *EZZ* (C_s, 37.5%), and *ZZZ* (C_{3v}, 12.5%).[9] Since each C_{3v} conformer (*EEE* and *ZZZ*) gives a single ^{1}H NMR signal for the three equivalent N-methyl groups and the C_s complexes (*EEZ*, *EZZ*) display two singlets in a 1:2 ratio, we expect six singlets for the methyl groups of L13 with relative intensities of 1:1:2:1:2:1 (statistical distribution). This is indeed experimentally observed for $[L13 - 3H]^{3-}$ in D_2O at pD = 10.0 (Figure 1a, the degree of protonation is justified in the next section),[20] and we deduce that the free energy difference between the conformers *EEE* (or *ZZZ*) and *EEZ* (or *EZZ)* has a pure entropic origin ($\Delta G^\circ = -RT \ln(3) = -2.7$ kJ/mol).[21] The lack of significant enthalpic contributions implies that the introduction of negatively charged carboxylate groups does not induce specific solvation processes or intramolecular interactions in $[L13 - 3H]^{3-}$.

Heating a solution of $[L13 - 3H]^{3-}$ in D_2O (pD = 10) at the highest accessible temperature (370 K) severely broadens the ^{1}H NMR signals, but coalescence of the singlets of the methyl groups occurs at 443 K in d_6-DMSO (dynamically averaged C_{3v} symmetry). Since all the possible interconversion processes *EEE* ↔ *EEZ* ↔ *EZZ* ↔ *ZZZ* coalesce within a small temperature range (438−443 K), a rough minimal energy barrier at this temperature of $\Delta G^\ddagger = 88(5)$ kJ/mol can be estimated by using the simplified Eyring equation, eq 1, which neglects the different populations of the exchangeable sites ($T_c = 443$ K is the coalescence temperature, $\delta\nu = 152$ Hz is the maximum frequency difference between the singlets of the methyl groups in the blocked conformers, k_B and h are the Boltzmann and Planck constants respectively).[22]

$$\Delta G^\ddagger = RT_c \ln\left(\frac{\sqrt{2}k_B}{\pi h}\frac{T_c}{\delta\nu}\right) = RT_c\left(22.96 + \ln\left(\frac{T_c}{\delta\nu}\right)\right) \quad (1)$$

This activation energy is typical for the hindered rotation of tertiary amides ($\Delta G^\ddagger = 86$ kJ/mol for *N*,*N*′-dimethylformamide),[23] and it is low enough to allow fast rearrangements compatible with the formation of thermodynamic products upon complexation with Ln(III).[21] A summary of the energetic profile of the exchange processes is given in the Supporting Information (Figure S1).

Acid−Base Constants of the Podand L13. Potentiometric titrations of L13 (10^{-3} M) with NaOH (0.05 M) in water/acetonitrile (95:5; 0.1 M $NaClO_4$) show two end points for NaOH/L13 = 2.0 and 3.0, in agreement with the three successive equilibria given in eqs 3−5 and $pK_a^2 \approx pK_a^3 \ll pK_a^4$. These potentiometric data can be satisfyingly fitted with nonlinear least-squares techniques to $pK_a^2 = 3.49(6)$, $pK_a^3 = 4.17(6)$ and $pK_a^4 = 6.19(3)$.

$$[L13 + H]^+ \rightleftharpoons [L13] + H^+ \quad K_a^1 \quad (2)$$

$$[L13] \rightleftharpoons [L13 - H]^- + H^+ \quad K_a^2 \quad (3)$$

$$[L13 - H]^- \rightleftharpoons [L13 - 2H]^{2-} + H^+ \quad K_a^3 \quad (4)$$

$$[L13 - 2H]^{2-} \rightleftharpoons [L13 - 3H]^{3-} + H^+ \quad K_a^4 \quad (5)$$

Reverse titrations with HCl (0.05−0.5 M; 0.1 M $NaClO_4$) confirm the values of pK_a^{2-4}, but they do not allow a precise determination of pK_a^1 in eq 2, which is too small to be experimentally accessible in these conditions ($pK_a^1 < 2.0$). For pH in the range 2.0−7.0, the calculated distribution curves predict complicated mixtures of species possessing variable degrees of protonation, but the totally deprotonated species $[L13 - 3H]^{3-}$ is quantitatively formed for pH ≥ 8.0 (Figure 2).

Parallel titrations of L13 (0.02 M) with NaOD in D_2O monitored by ^{1}H NMR are restricted to $5 \le pD \le 10$[20] because of the limited solubility of the ligand. For pD ≥ 8, the deprotonated podand $[L13 - 3H]^{3-}$ is quantitatively formed and exists as a statistical mixture of its four conformers (*EEE*, *EEZ*, *EZZ*, *ZZZ*) as previously discussed (Figure 1a). At pD = 5.2, the monoprotonated podand $[L13 - 2H]^{2-}$ dominates the ^{1}H NMR spectrum (84%) which still

(20) pD = pH + 0.4. Glasoe, P. K.; Long, F. A. *J. Phys. Chem.* **1960**, *64*, 188.
(21) Renaud, F.; Decurnex, C.; Piguet, C.; Hopfgartner, G. *J. Chem. Soc., Dalton Trans.* **2001**, 1863.
(22) Pons, M.; Millet, O. *Prog. Nucl. Magn. Reson. Spectrosc.* **2001**, *38*, 267.
(23) Günther, H. *NMR Spectroscopy*; John Wiley & Sons: Chichester, U.K., 1980; p 244.

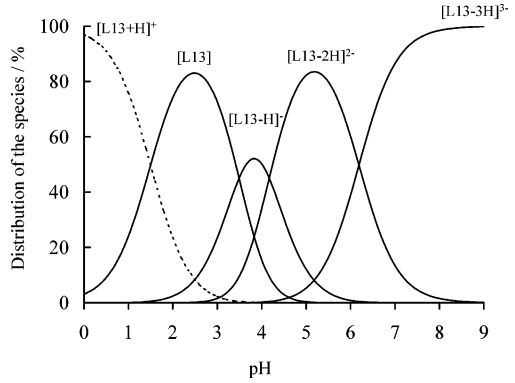

Figure 2. Distribution curves for the podands $[L13 - iH]^{i-}$ ($i = -1$, 0, 1, 2, 3) versus pH calculated with eqs 2−5 and pK_a^1 taken as equal to 1.5 (water/acetonitrile = 95:5; 0.1 M $NaClO_4$).

displays six singlets for the methyl groups compatible with an approximate statistical mixture of the four conformers (Figure 1b). However, the multiplets assigned to the protons of the ethylene spacers are shifted downfield upon protonation ($\delta = 2.1-3.4$ ppm in $[L13 - 3H]^{3-}$, $\delta = 3.3-3.9$ ppm in $[L13 - 2H]^{2-}$, Figure 1). This is diagnostic for the protonation of the apical nitrogen atom in L13 which produces a strong electron-withdrawing effect within the Me−TREN cap.[9,24] We conclude that (i) the apical nitrogen is selectively protonated in $[L13 - 2H]^{2-}$ and (ii) the isolated neutral ligand L13 corresponds to a zwitterionic form in which one carboxylato−pyridine group is deprotonated. This behavior closely parallels that reported for the shorter analogue $[L14 - 3H]^{3-}$ for which the protonation of the apical nitrogen occurs at $pK_a^4 = 6.78(4)$,[25] while the macroscopic equilibrium constants[26] for the carboxylato−pyridine groups amount to $pK_a^3 = 4.11(6)$, $pK_a^2 = 3.3(1)$, and $pK_a^1 = 2.5(2)$. Although the deprotonation constant of the apical nitrogen atom in $[L13 - 2H]^{2-}$ ($pK_a^4 = 6.19(3)$) agrees with $pK_a = 6.36-6.44$ previously reported for a similar TREN tripod connected to monoanionic sidearms via amide linkers,[27] it significantly differs from $pK_a = 4.66(2)$ found for $[L8 + H]^+$ in the same conditions.[9] The overall negative charge of $[L13 - 3H]^{3-}$ may partially account for the increased basicity of the nitrogen cap, but the formation of intramolecular bifurcated and trifurcated NH···OC hydrogen bonds evidenced in $[L8 + H]^+$ [9] has no counterpart in $[L13 - 2H]^{2-}$.

Formation and Stability of the Podates [Ln(L13 − 3H)] in Solution (Ln = La−Lu). To avoid competitive protonation equilibria, the complexation process has been investigated in buffered solution at pH = 8 (tris(hydroxymethyl)-aminomethane−HCl, 0.05 M) where (i) $[L13 - 3H]^{3-}$ is quantitatively formed in solution (Figure 2) and (ii) the hydrolysis of Ln(III) is limited to the first hydrolytic equilibrium ($pK_a^{1,Ln} = 9.01-7.90$, Ln = La−Lu).[4c] Since

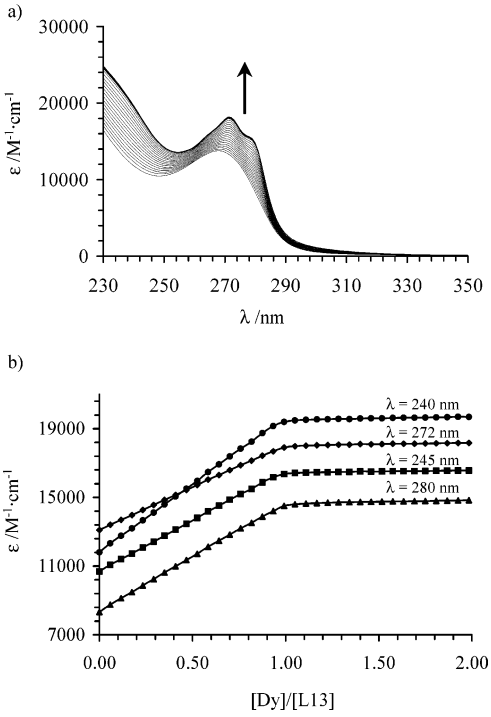

Figure 3. (a) Variation of the absorption spectra observed for the spectrophotometric titration of $[L13 - 3H]^{3-}$ (10^{-4} M in water, pH = 8) with $Dy(ClO_4)_3 \cdot H_2O$ at 298 K (Dy/L13 = 0.1−2.0). (b) Corresponding variation of observed molar extinctions at four different wavelengths.

the intrinsic basicity of the capping nitrogen atom is reduced when the three tridentate sidearms are coordinated to Ln^{3+} ($pK_a([Ln(L8 + H)]^{4+}) = 3.5(2)$ compared with $pK_a([L8 + H]^+) = 4.66(2)$ in the same conditions),[9] the final podate [Ln(L13 − 3H)] is expected to be quantitatively deprotonated in these conditions. Spectrophotometric titrations of $[L13 - 3H]^{3-}$ in water (10^{-4} M, pH = 8.0) with $Ln(ClO_4)_3 \cdot xH_2O$ (Ln = La−Lu, $x = 6-8$) display a smooth end point for Ln/L13 = 1.0 in agreement with the formation of the 1:1 podates [Ln(L13−3H)] (Figure 3). Factor analysis[28] systematically confirms the formation of a single absorbing complex (Ln = La−Lu), and the spectrophotometric data can be satisfyingly fitted with nonlinear least-squares techniques[29] to eq 6 with the apparent formation constants $\log(\beta_{110,apparent}^{Ln})$ collected in Table 1.

$$Ln(III)_{tot} + [L13 - 3H]^{3-} \rightleftharpoons [Ln(L13 - 3H)] \quad \beta_{110,apparent}^{Ln} \quad (6)$$

Since $Ln(III)_{tot}$ exists as a mixture of Ln^{3+} and $[Ln(OH)]^{2+}$ at pH = 8, the conditional formation constants β_{110}^{Ln} defined in eq 7[26] and the apparent constants $\beta_{110,apparent}^{Ln}$ are related by $\beta_{110}^{Ln} = \beta_{110,apparent}^{Ln} \cdot((|H^+| + K_a^{1,Ln})/|H^+|)$,[24,26] in which $K_a^{1,Ln}$ is the first hydrolysis constant for each lanthanide.[4c]

$$Ln^{3+} + [L13 - 3H]^{3-} \rightleftharpoons [Ln(L13 - 3H)] \quad \beta_{110}^{Ln} \quad (7)$$

(24) Xu, J.; O'Sullivan, B.; Raymond, K. N. *Inorg. Chem.* **2002**, *41*, 6731.
(25) Bretonnière, Y.; Mazzanti, M.; Pécaut, J.; Dunand, F. A.; Merbach, A. E. *Inorg. Chem.* **2001**, *40*, 6737.
(26) Kiss, T.; Sovago, I.; Martin, R. B. *Polyhedron* **1991**, *10*, 1401 and references therein.
(27) Serratrice, G.; Boukhalfa, H.; Béguin, C.; Baret, P.; Caris, C.; Pierre, J.-L. *Inorg. Chem.* **1997**, *36*, 3898.
(28) Malinowski, E. R.; Howery, D. G. *Factor Analysis in Chemistry*; Wiley: New York, 1980.
(29) (a) Gampp, H.; Maeder, M.; Meyer, C. J.; Zuberbühler, A. D. *Talanta* **1986**, *33*, 943. (b) Gampp, H.; Maeder, M.; Meyer, C. J.; Zuberbühler, A. D. *Talanta* **1985**, *23*, 1133.

Table 1. Apparent Formation Constants $\log(\beta^{Ln}_{110,apparent})$ and Calculated Conditional Formation Constants $\log(\beta^{Ln}_{110})^a$ for the Complexes [Ln(L13 − 3H)] in Water (pH = 8, 298 K)

Ln	$\log(\beta^{Ln}_{110,apparent})$	$pK_a^{1,Ln}$ [b]	$\log(\beta^{Ln}_{110})$
La	6.8 ± 0.1	9.01	6.8 ± 0.1
Nd	6.6 ± 0.2	8.43	6.7 ± 0.2
Sm	6.7 ± 0.2	8.34	6.9 ± 0.2
Gd	6.5 ± 0.2	8.35	6.7 ± 0.2
Dy	6.5 ± 0.2	8.10	6.8 ± 0.2
Ho	6.7 ± 0.2	8.04	7.0 ± 0.2
Er	6.5 ± 0.2	7.99	6.8 ± 0.2
Tm	6.6 ± 0.2	7.95	6.9 ± 0.2
Lu	6.6 ± 0.2	7.90	7.0 ± 0.2

[a] $\beta^{Ln}_{110} = \beta^{Ln}_{110,apparent} \times ((|H^+| + K_a^{1,Ln})/|H^+|)$, see text. [b] Taken from ref 4c.

The calculated $\log(\beta^{Ln}_{110})$ values only marginally deviate from $\log(\beta^{Ln}_{110,apparent})$ at pH = 8 and do not significantly vary from their average value ($\log(\beta^{Ln}_{110})$ = 6.8(3)). This points to the absence of pronounced size-discriminating effect along the lanthanide series (Table 1). The $\log(\beta^{Ln}_{110})$ value for [Ln(L13 − 3H)] can be compared with $\log(\beta^{Ln}_{110})$ = 5.0−7.5 reported for $[Ln(L8)]^{3+}$ in acetonitrile/water (95:5),[9] a much less competing solvent. In pure water, $[Ln(L8)]^{3+}$ is quantitatively dissociated which demonstrates the beneficial effect of the terminal carboxylate group for the stabilization of nine-coordinate podates. Interestingly, the heptadentate podand $[L14 - 3H]^{3-}$ produces even more stable podates ($\log(\beta^{Ln}_{110})$ = 10.2(2) for [Gd(L14 − 3H)-$(OH_2)_3$] in water)[25] despite the formation of only three five-membered chelate rings in [Ln(L14 − 3H)$(OH_2)_3$] instead of six for [Ln(L13−3H)]. This suggests that the formation of three supplementary Ln−O carboxamide bonds combined with the larger chelate effect expected in [Ln(L13−3H)] does not overcome the extra free energy required for removing the remaining solvent molecules in nine-coordinate podates.

As a result of the charge compensation occurring upon complexation of Ln^{3+} with $[L13 - 3H]^{3-}$, the neutral podates [Ln(L13 − 3H)] display no affinity for a second ligand, which contrasts with the detection of $[Ln(L8)_2]^{3+}$ for Ln = La−Pr.[9] However, this charge compensation concomitantly limits solvation in polar solvents, and [Ln(L13 − 3H)] is poorly soluble in water (maximum solubility ≈ 10^{-4} M), which prevents the use of NMR or potentiometric techniques for characterizing the complexation process in solution.

Isolation of the Podates [Ln(L13 − 3H)] in the Solid State (Ln = Eu, Gd, Tb, Lu). The mixing of stoichiometric quantities of $[L13 - 3H]^{3-}$ and $Ln(ClO_4)_3 \cdot xH_2O$ (Ln = Eu, Gd, Tb, Lu, x = 6−8) in water at pH = 8.0 (NaOH) produces clear solutions from which microcrystalline complexes [Ln(L13 − 3H)]$\cdot xH_2O$ (Ln = Eu, x = 4.4, **4**; Gd, x = 6.5, **5**; Tb, x = 7.3, **6**; Lu, x = 3.8, **7**) precipitate in fair yields (65−80%). The IR spectra show the characteristic ligand vibrations together with a strong broad band envelope at 1620 cm^{-1} assigned to ν(C═O). No peak corresponding to perchlorate anions can be detected in agreement with a quantitative deprotonation of the final podate. Fragile X-ray quality prisms of [Ln(L13 − 3H)]$\cdot 7H_2O$ (Ln = Eu, **8**; Tb, **9**; Lu, **10**) are obtained by slow evaporation of diluted water solutions of **4**, **6**, and **7**, respectively. A direct transfer of the crystals from the mother liquor onto the diffractometer avoids water loss and decomposition.

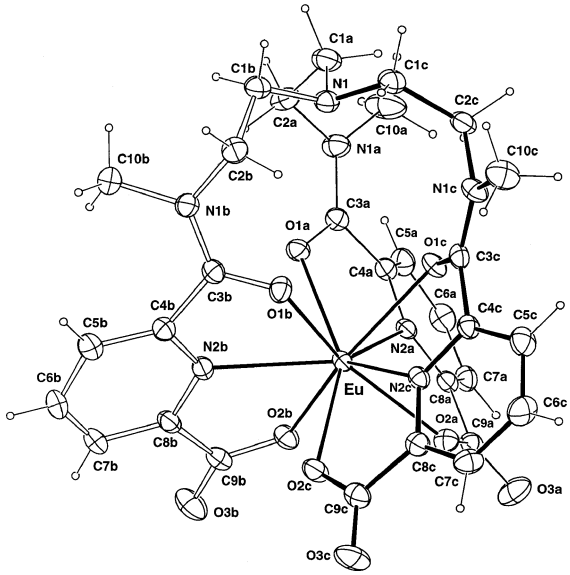

Figure 4. ORTEP view perpendicular to the pseudo-C_3 axis with the atomic numbering scheme for the complex [Eu(L13 − 3H)] in **8**. Ellipsoids are represented at the 40% probability level. This atomic numbering scheme also holds for complexes **9** and **10**.

Crystal and Molecular Structures of the Podates [Ln(L13 − 3H)]$\cdot 7H_2O$ (Ln = Eu, Tb, Lu). The complexes [Ln(L13 − 3H)]$\cdot 7H_2O$ (Ln = Eu, **8**; Tb, **9**; Lu, **10**) are isostructural and show a neutral podate [Ln(L13 − 3H)] in the asymmetric unit together with seven interstitial water molecules, of which one is disordered (O7w, see Experimental Section). The water molecules are involved in 11 hydrogen bonds according to the loose structural criteria D···A ≤ 3.1 Å and D−H···A ≥ 120° (Table S1, Supporting Information).[30] No water molecule is located in the first coordination sphere, but the neutral complex [Ln(L13 − 3H)] participates in four hydrogen bonds in which the noncoordinated oxygen atoms O3 of each terminal carboxylate group interact with the water molecules O1w, O2w, O6w, and O7w (Table S1, Supporting Information). The podates [Ln(L13 − 3H)] are arranged in columns along the [100] direction in the crystal and display π-stacking interactions between the pyridine rings of ligand strands a and c of one complex with the parallel pyridine rings of neighboring complexes related by inversion centers (interplanar distances 3.30 and 3.45 Å, Figure S2, Supporting Information). Since the carboxylate groups are nonbridging, the neutral podates [Ln(L13 − 3H)] can be considered as monomeric units. Figure 4 shows the numbering scheme for the podates [Ln(L13 − 3H)], and selected bond distances and angles are given in Table 2 (complete data for the coordination spheres and least-squares plane data are given in Tables S2−S5, Supporting Information).

Each unsymmetrical carboxamide−pyridine−carboxylate tridentate binding unit is tricoordinated to Ln(III) and helically wrapped about a pseudo-C_3 axis passing through N1 and Ln (Figure 5). The coordination sphere of the nine-

(30) Steiner, T. *Angew. Chem., Int. Ed.* **2002**, *41*, 48 and references therein.

Table 2. Selected Bond Lengths [Å] and Bond Angles [deg] in [Ln(L13 − 3H)]·7H_2O (Ln = Eu, **8**; Tb, **9**; Lu, **10**)

Bond Distances

	strand a			strand b			strand c		
	8	**9**	**10**	**8**	**9**	**10**	**8**	**9**	**10**
Ln−O1	2.463(2)	2.443(2)	2.391(3)	2.459(2)	2.440(2)	2.381(3)	2.442(2)	2.422(2)	2.368(3)
Ln−O2	2.449(2)	2.424(2)	2.355(3)	2.399(3)	2.375(2)	2.316(3)	2.431(3)	2.411(2)	2.348(3)
Ln−N2	2.544(3)	2.522(2)	2.453(4)	2.517(3)	2.489(2)	2.423(4)	2.528(3)	2.504(2)	2.436(3)
Ln···N1	4.786(3)	4.795(3)	4.798(4)						

Bite Angles

	strand a			strand b			strand c		
	8	**9**	**10**	**8**	**9**	**10**	**8**	**9**	**10**
O1−Ln−O2	126.48(7)	127.58(7)	129.9(1)	128.11(9)	129.14(7)	131.6(1)	127.43(8)	128.37(7)	130.9(1)
O1−Ln−N2	62.95(8)	63.53(7)	64.6(1)	63.83(9)	64.36(8)	65.6(1)	63.19(9)	63.82(7)	65.0(1)
O2−Ln−N2	63.59(8)	64.11(7)	65.3(1)	64.28(9)	64.77(8)	66.1(1)	64.25(9)	64.57(7)	65.9(1)

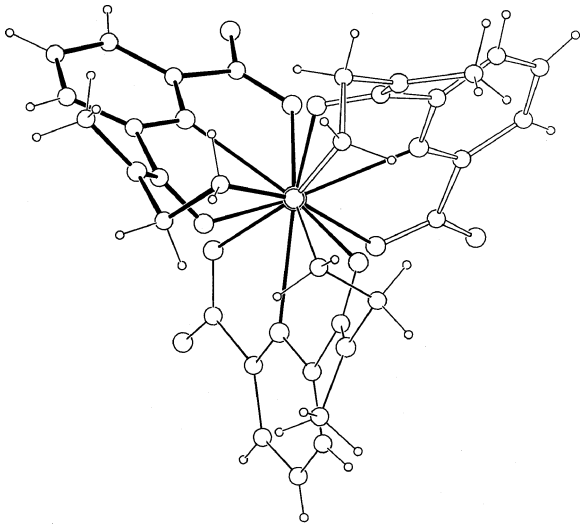

Figure 5. Perspective view of [Eu(L13 − 3H)]·7H_2O along the pseudo-C_3 axis showing the helical twist of the complex.

coordinate Ln(III) is best described as a distorted tricapped trigonal prismatic site in which the three carboxamide oxygen atoms (O1a, O1b, O1c) and the three carboxylate oxygen atoms (O2a, O2b, O2c) define the two trigonal faces of the prisms (F3 = {O1a, O1b, O1c}, F5 = {O2a, O2b, O2c}, while the three pyridine nitrogen atoms (N2a, N2b, N2c) form an intermediate plane (F4 = {N2a, N2b, N2c}) which almost contains Ln(III) (deviation: 0.046 Å (Ln = Eu, **8**), 0.038 Å (Ln = Tb, **9**), 0.029 Å (Ln = Lu, **10**) toward F3). The Eu−N(pyridine), Eu−N(carboxamide), and Eu−N(carboxylate) bond distance are similar to those found in closely related nine-coordinate complexes (Table 3).[9,10,13,31] Interestingly, the average Eu−O(carboxamide) bond distance in [Eu(L13 − 3H)] (2.45(1) Å) is only marginally longer than the average Eu−O(carboxylate) bond distance (2.43(1) Å) in agreement with a faint effect of the negative charge borne by the carboxylate on the Eu−O bond strength. The effective ionic radii calculated according to Shannon's definition[32] for [Ln(L13 − 3H)] with r(N) = 1.46 Å and r(O) = 1.31 Å amount to $R_{Eu(III)}$ = 1.11 Å (expected 1.120 Å),[32] $R_{Tb(III)}$ = 1.09 Å (expected 1.095 Å),[32] and $R_{Lu(III)}$ = 1.03 Å (expected 1.032 Å),[32] which demonstrates that (i) the cavity of the podate can be easily adapted for the lanthanide contraction and (ii) the covalent tripod does not induce specific sterical contraints affecting the helical wrapping.

The triple-helical [Ln(L13 − 3H)] podates adopt cylindrical shapes displaying similar nonbonding O···O distances between the oxygen atoms of each of the trigonal faces F3 and F5 (F3, O1*i*···O1*j* = 2.98−3.07 Å; F5, O2*i*···O2*j* = 3.04−3.12 Å in [Eu(L13 − 3H)]) as found in the nonclipped analogue $[Eu(L2)_3]^{3+}$ (O1*i*···O1*j* = 2.97−3.14 Å)[5a], but in contrast with the conical shape reported for $[Eu(L8 + H)]^{4+}$ (F3, O1*i*···O1*j* = 2.80 Å; F5, O2*i*···O2*j* = 3.01Å).[9] We can now safely assign the latter distortion to the existence of an intramolecular trifurcated hydrogen bond in $[Eu(L8 + H)]^{4+}$ which involves the protonated apical nitrogen atom (donor) and the oxygen atoms (acceptors) of the upper trigonal F3 face. A detailed structural analysis of the coordination sphere based on the ϕ (bending), θ_t (flattening), and ω_t (torsion) angles shows a regular arrangement of the six oxygen donors which are close to an ideal trigonal prism (Table S6, Supporting Information).[5a,33] However, the two trigonal faces are offset by ω = 15° in [Eu(L13 − 3H)] (ideal prism ω = 0°, ideal octahedron ω = 60°) as similarly found for the nonclipped analogues $[Eu(L2)_3]^{3+}$ (ω = 16°) and $[Eu(L1 - 2H)_3]^{3-}$ (ω = 18°).[5a] This distortion decreases for smaller Ln(III) (ω = 14° for [Tb(L13 − 3H)] and ω = 11° for [Lu(L13 − 3H)]) in agreement with a tighter wrapping of the helical strands about the pseudo-C_3 axis. A quantitative structural analysis of the helical revolution of the ligand threads in [Ln(L13 − 3H)] requires the use of the five facial planes F1−F5 defined by the atoms of each strand related by the pseudo-C_3 axis. The coordination sphere around Ln(III) is thus sliced into two helical portions delimited by the facial planes F5 = {O2a, O2b, O2c}, F4 = {N2a, N2b, N2c}, and F3 = {O1a, O1b, O1c}, while the covalent tripod is characterized by two helical portions delimited by F3, F2 = {C2a, C2b, C2c}, and F1 = {C1a, C1b, C1c} (Figure 4). These facial planes are almost parallel (dihedral angles 0−2° Tables S3−S5, Supporting Information) and separated by interplanar distances d_{ij} which correspond to the linear progression of the strand along the helical axis within each

(31) Calculated from the crystal structure of [Sm(L11 − 3H)][12] after correction for the change in ionic radii.[32]

(32) Shannon, R. D. *Acta Crystallogr.* **1976**, *A32*, 751.

(33) Piguet, C.; Bünzli, J.-C. G.; Bernardinelli, G.; Bochet, C. G.; Froidevaux, P. *J. Chem. Soc., Dalton Trans.* **1995**, 83.

Table 3. Comparisons of Average Eu−N(pyridine), Eu−O(carboxamide), and Eu−O(carboxylate) Bond Lengths [Å] Observed in [Eu(L13 − 3H)]·7H$_2$O (**8**) and Related Nine-Coordinate Complexes

complex	Eu−N(pyridine)	Eu−O(carboxamide)	Eu−O(carboxylate)	ref
[Eu(L13 − 3H)]	2.53(1)	2.45(1)	2.43(1)	this work
[Eu(L8 + H)]$^{4+}$	2.568(7)	2.40(1)		9
[Eu(L2)]$^{4+}$	2.56(1)	2.41(1)		5a
[Eu(L9)]$^{3+}$	2.60(1)	2.3945(5)		10
[Eu(L12 − 2H)]$^{+}$	2.62(6)		2.38(1)	13
[Eu(L11 − 3H)]			2.383(5)	31

Table 4. Helical Pitches P_{ij} (Å), Linear Distances d_{ij} (Å), and Average Twist Angle ω_{ij} (deg) along the Pseudo-C_3 Axis in [Ln(L13 − 3H)]·7H$_2$O (Ln = Eu, **8**; Tb, **9**; Lu, **10**) and [Eu(L8 + H)](CF$_3$SO$_3$)$_3$(PF$_6$)(CH$_3$CN)$_{0.5}$[a]

	[Eu(L13−3H)] (**8**)			[Tb(L13−3H)] (**9**)			[Lu(L13−3H)] (**10**)			[Eu(L8+H)]$^{4+}$ [b]		
helical portion	d_{ij}	ω_{ij}	P_{ij}	d_{ij}	ω_{ij}	P_{ij}	d_{ij}	ω_{ij}	P_{ij}	d_{ij}	ω_{ij}	P_{ij}
F1−F2[c]	0.89	20	16.0	0.91	20	16.2	0.93	20	16.7	0.58	25	8.4
F2−F3	2.65	7	136.3	2.65	7	136.1	2.64	7	135.9	2.49	7	128.3
F3−F4	1.67	53	11.4	1.67	53	11.4	1.66	54	11.1	1.81	48	13.6
F4−F5	1.69	52	11.7	1.67	53	11.4	1.64	55	10.7	1.62	52	11.2

[a] Each helical portion Fi−Fj is characterized by (i) a linear extension d_{ij} defined by the separation between the facial planes, (ii) an average twist angle ω_{ij} defined by the angular rotation between the projections of Oi and Nj (or Cj) belonging to the same ligand strand, and (iii) its pitch P_{ij} defined as the ratio of axial over angular progressions along the helical axis (see text). [b] Calculated from the crystal structure reported in ref 9. [c] F1 = {C1a, C1b, C1c}, F2 = {C2a, C2b, C2c}, F3 = {O1a, O1b, O1c}, F4 = {N2a, N2b, N2c}, F5 = {O2a, O2b, O2c}.

part limited by Fi and Fj (Table 4). The ω_{ij} angles between the projections of the X_i and Y_j atoms of the same strand belonging to the different planes Fi and Fj measure the angular rotation.[9] The pitch of each helical portion can then be calculated according to $P_{ij} = (d_{ij}/\omega_{ij})360$ (Table 4, P_{ij} corresponds to the length of a cylinder containing a single turn of the helix defined by the geometrical characteristics d_{ij} and ω_{ij}).[9,11]

The helical twist of the tridentate binding units defined by F4−F5 and F3−F4 is regular, and the associated pitches P_{45} = 11.7 Å and P_{34} = 11.4 Å for [Eu(L13 − 3H)] are comparable with those found in [Eu(L8 + H)]$^{4+}$ (P_{45} = 11.2 Å and P_{34} = 13.6 Å)[9] except for the slight constraint imposed by the trifurcated hydrogen bonding in the F3−F4 portion of the latter complex. The helical twist smoothly increases with the decreasing size of Ln(III) and reaches P_{45} = 10.7 Å and P_{34} = 11.1 Å for [Lu(L13 − 3H)]. The helix abruptly stops within the F2−F3 portion (P_{23} = 135.9−136.3 Å) and reverses its screw direction in the short terminal helical F1−F2 portion (P_{12} = 16.0−16.7 Å). A similar behavior is observed for the analogous podate [Eu(L8 + H)]$^{4+}$ with P_{23} = 128.3 Å and P_{12} = 8.4 Å,[9] but the smaller value found for P_{12} results from the flattening of the covalent tripod associated with the trifurcated hygrogen bond (Eu···N1 = 4.33(1) Å for [Eu(L8 + H)]$^{4+}$ compared with 4.795(3) Å for [Eu(L13 − 3H)]). We conclude that, contrary to our original suggestion,[9] no strong sterical constraints are induced within the short covalent Me−TREN tripod in L8 and L13, and a regular helication of the three unsymmetrical tridentate pyridine-containing strands around nine-coordinate Ln(III) is observed along the complete lanthanide series. However, the replacement of terminal carboxamide groups with carboxylates in [Eu(L13 − 3H)] induces negligible structural changes in the coordination sphere (Figure S3, Supporting Information).

Electronic and Photophysical Properties of the Podates [Ln(L13 − 3H)]·xH$_2$O (Ln = Eu, x = 4.4, 4; Gd, x = 6.5, 5; Tb, x = 7.3, 6; Lu, x = 3.8, 7). Ligand-Centered Excited States. In water, the ligand [L13 − 3H]$^{3-}$ shows a broad and asymmetric absorption band envelope centered around 37310 cm^{-1} and assigned to a combination of $n \rightarrow \pi^*$ and $\pi \rightarrow \pi^*$ transitions as previously established for L2 (37040 cm^{-1})[5a] and L8 (37450 cm^{-1}).[9] Upon complexation to Ln(III), the broad absorption becomes structured with (i) a red-shift of the maximum (36700 cm^{-1}, $\Delta\nu$ = 610 cm^{-1}; Ln = La−Lu), (ii) a slight increase in intensity, and (iii) the appearance of shoulders on both high (37300 cm^{-1}) and low (35700 cm^{-1}) energy sides (Table 5). A parallel behavior is observed for L13 in the solid state (Table 5), and excitation via the ligand-centered excited states (77 K, $\tilde{\nu}_{exc}$ = 36765 cm^{-1}) produces a well-resolved fluorescence spectrum originating from the $^1\pi\pi^*$ level (0−0 phonon, 22460 cm^{-1}). Time-resolved spectra (delay times 10−100 μs) show a faint residual long-lived emission at the same energy originating from the $^3\pi\pi^*$ level (0−0 phonon at 22070 cm^{-1}; biexponential decay, τ_1 = 146(2) ms and τ_2 = 5.9(2) ms). Similar emission characteristics are obtained for the coordinated ligand in the diamagnetic complex [Lu(L13 − 3H)] (**7**) except for a shorter $^3\pi\pi^*$ lifetime (biexponential decay: τ_1 = 27(1) ms and τ_2 = 5.5(1) ms, Table 5, Figure 6a) resulting from the partial mixing of ligand-centered singlet and triplet wave functions induced by the heavy Lu(III) atom.[34]

For the paramagnetic complex [Gd(L13 − 3H)] (**5**), the metal-centered excited levels are too high to be accessible for intramolecular energy transfers from the $^1\pi\pi^*$ or $^3\pi\pi^*$ levels,[35] but the Coulomb interactions between the electrons of the podand and the metal ion further mix the ligand-centered triplet and singlet wave functions which reduces the $^3\pi\pi^*$ lifetime (biexponential decay, τ_1 = 3.05(2) ms and τ_2 = 0.66(1) ms, Table 5, Figure 6b).[34] Consequently, the

(34) (a) Tobita, S.; Arakawa, M.; Tanaka, I. *J. Phys. Chem.* **1984**, *88*, 2697. (b) Tobita, S.; Arakawa, M.; Tanaka, I. *J. Phys. Chem.* **1985**, *89*, 5649.
(35) Carnall, W. T.; Fields, P. R.; Rajnak, K. *J. Chem. Phys.* **1968**, *49*, 4443.

Table 5. Ligand-Centered Absorption at 295 K and Emission Properties at 77 K for the Ligand L13 and Selected Complexes [Ln(L13 − 3H)]·xH$_2$O (Ln = Eu, x = 4.4, **4**; Gd, x = 6.5, **5**; Tb, x = 7.3, **6**; Lu, x = 3.8, **7**) in the Solid State

compd	$E(\pi,n \rightarrow \pi^*)$/cm^{-1} [a]	$E(\pi,n \rightarrow \pi^*)$/cm^{-1} [b]	$E(^1\pi\pi^*)$/cm^{-1} [c]	$E(^3\pi\pi^*)$/cm^{-1} [c]	$\tau(^3\pi\pi^*)$/ms	
$(L13 - 3H)^{3-}$	37310 (14000)	35210 (broad)	22460	22070 (sh)	146(2)	5.9(2)
			20620			
			18800			
			16900			
[Eu(L13 − 3H)]	37300 (16060sh)	34710 (broad)	23680	*d*		
	36630 (17380)	32260 (sh)				
	35710 (14960sh)					
[Gd(L13 − 3H)]	37300 (17200sh)	34700 (broad)	23710	23000	3.05(2)	0.66(1)
	36760 (18250)	31750 (sh)	22270			
	35840 (15450sh)		20580			
			18830			
[Tb(L13 − 3H)]	37300 (17000sh)	34710 (broad)	23640	*d*		
	36630 (17800)	32000 (sh)				
	35710 (14800sh)					
[Lu(L13 − 3H)]	37300 (16900sh)	35200 (broad)	23500	22600	27(1)	5.5(1)
	36630 (18300)	32300 (sh)				
	35590 (15100sh)					

[a] 10^{-4} M in water, at pH 8; sh = soulder. Energies are given for the maximum of the band envelope, and the molar absorption coefficient (ϵ) is given in parentheses in M^{-1}·cm^{-1}. [b] Reflectance spectra in the solid state. [c] Data obtained from the emission spectra at 77 K. [d] Quenched by efficient L13($^3\pi\pi^*$) → Ln(III) transfer.

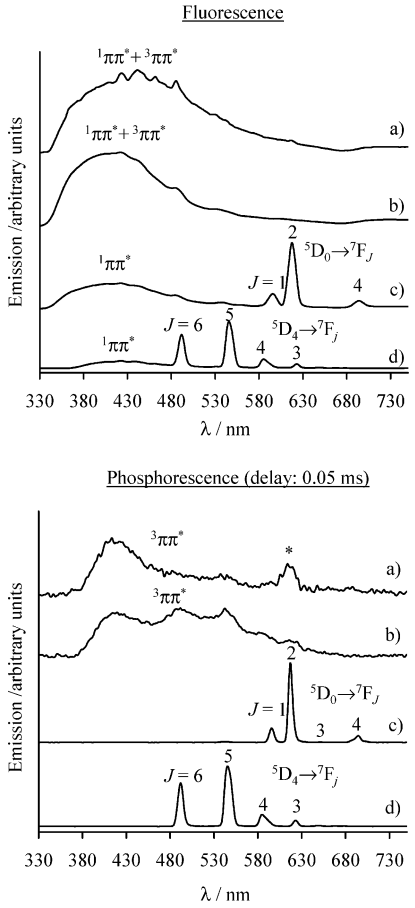

Figure 6. Fluorescence (top) and associated time-resolved phosphorescence (bottom) spectra of (a) [Lu(L13 − 3H)] (asterisk (*) indicates traces of Eu(III)), (b) [Gd(L13 − 3H)], (c) [Eu(L13 − 3H)], and (d) [Tb(L13 − 3H)]; $\tilde{\nu}_{exc}$ = 36765 cm^{-1}, 77 K, 0.05 ms delay for phosphorescence spectra.

radiative emission of the spin-forbidden $^3\pi\pi^*$ level becomes more efficient,[34] and the emission spectrum of **5** at 77 K displays the expected $^1\pi\pi^*$ fluorescence at 23710 cm^{-1} together with a significant $^3\pi\pi^*$ emission at 23000 cm^{-1} (0−0 phonon). This standard photophysical ligand-centered behavior[11] observed for L13 and its complexes [Ln(L13 − 3H)] (Ln = Gd, Lu) strongly contrasts with the undetectable emission reported for the analogous podand L8 and the faint $^1\pi\pi^*$ emission detected for [Gd(L8)](CF$_3$SO$_3$)$_3$ at high energy (0−0 phonon at 25000 cm^{-1}) in the same conditions (the emission of $^3\pi\pi^*$ was too weak to be detected).[9] The improved emissive properties of L13 and of its complexes **5** and **7** compared to L8 and its Lu- and Gd-podates can be tentatively assigned to the replacement of carboxamide groups with carboxylates which (i) increases the rigidity of the complex via the participation in intermolecular hydrogen bonds and (ii) removes vibrational quenching due to high-frequency CH bonds of the diethylamide residue.[36] However, the origin of the 2000 cm^{-1} blue shift of the $^1\pi\pi^*$ level in [Gd(L8)](CF$_3$SO$_3$)$_3$ and the faint singlet−triplet energy gap in [Gd(L13 − 3H)] (ΔE_{S-T} = 710 cm^{-1}) remain obscure and deserve to be addressed for the design of rational L → Ln energy transfer processes.

Theoretical Modeling of Ligand-Centered Excited States in L8 and L13. We have performed time-dependent DFT (TDDFT) calculations in order to unravel the electronic structure and the energy levels of the lowest ligand-centered singlet and triplet excited states. Since (i) the three tridentate binding units in L8 and L13 are connected by a Me−TREN spacer which is a poor electronic relay and (ii) the Ln−ligand bonds are mainly electrostatic,[37] the TDDFT calculations have been restricted to a single tridentate binding unit corresponding to one noncoordinated ligand strand taken from the molecular structures of [Eu(L8 + H)](CF$_3$SO$_3$)$_3$-(PF$_6$)(CH$_3$CN)$_{0.5}$[9] (binding unit A) and [Eu(L13 − 3H)]·7H$_2$O (**8**, binding unit B). Figures 7 and 8 show the binding units together with selected Kohn−Sham orbitals lying close to the HOMO−LUMO gap. The associated computed energies for the 50 lowest singlet and triplet excited states are given in Tables S7 and S8 (Supporting Information).

(36) Beeby, A.; Clarkson, I. M.; Dickins, R. S.; Faulkner, S.; Parker, D.; Royle, L.; de Sousa, A. S.; Williams, J. A. G.; Woods, M. *J. Chem. Soc., Perkin Trans. 2* **1999**, 493.
(37) Kaltsoyannis, N.; Scott, P. *The f-Elements*; Oxford University Press: Oxford, 1999.

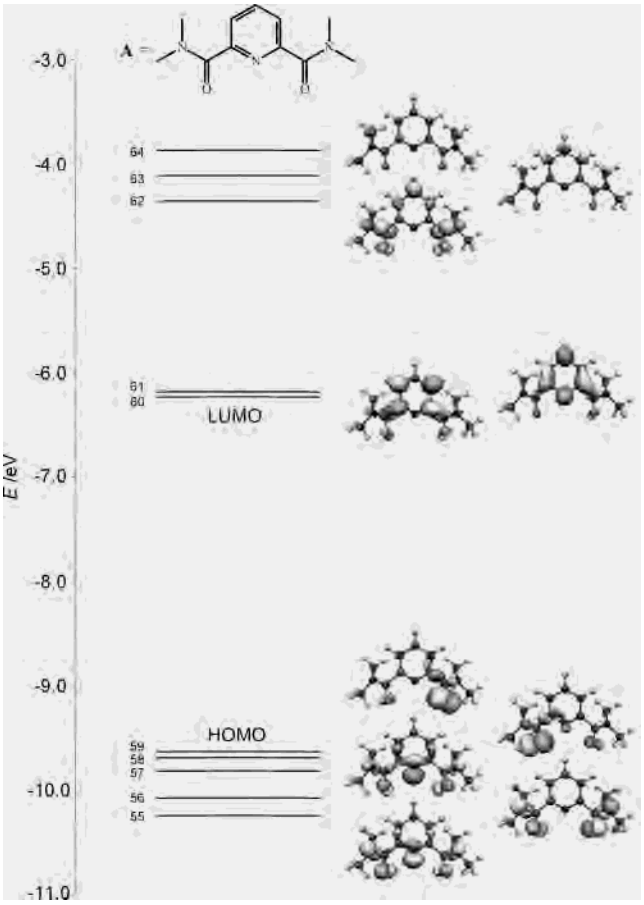

Figure 7. Selected Kohn−Sham orbitals close to the HOMO−LUMO gap for the tridentate binding unit A in $[Eu(L8 + H)]^{4+}$.

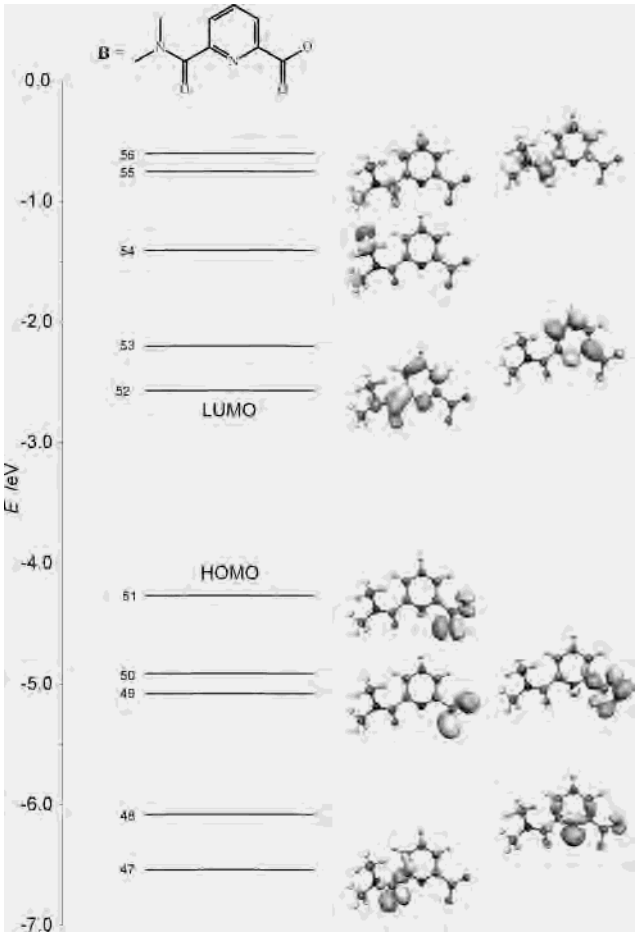

Figure 8. Selected Kohn−Sham orbitals close to the HOMO−LUMO gap for the tridentate binding unit B in [Eu(L13 − 3H)].

The HOMO and the next lowest occupied orbital (SHOMO) in A and B correspond to nonbonding (or poorly bonding) π orbitals centered on the terminal carboxamide (A) or on the carboxylate (B) moieties (approximately located in the pyridine plane). Since the negative carboxylate in B is easier to oxidize than the neutral carboxamide in A, the HOMO and SHOMO are expected (and calculated) at higher energies for B. On the other hand, the LUMO orbitals for A and B correspond to π-antibonding orbitals centered on the pyridine ring (perpendicular to the aromatic ring) and involving only a limited participation of the sidearms. Since the carboxylate group is a weaker electron-withdrawing substituent (Hammett coefficient $\sigma_p = 0.00$)[38] than the carboxamide (Hammet coefficient $\sigma_p = 0.36$),[38] we expect (and calculate) lower energies for the π^* orbitals centered on the pyridine ring of A. If we restrict the discussion to the lowest ligand-centered excited states experimentally accessible in the emission spectra, we can simply consider the transfer of one electron from the HOMO to the LUMO. According to Figures 7 and 8, this transition occurs at a significantly lower energy for B and exhibits a considerable charge-transfer character (sidearms → pyridine). This rough theoretical model qualitatively agrees with the considerable red-shift ($\approx$2000 cm^{-1}) observed for the $^1\pi\pi^*$ emission when going from $[Gd(L8)]^{3+}$ (terminal carboxamide, unit A) to [Gd(L13 − 3H)] (terminal carboxylate, unit B). Regarding the lowest open-shell triplet state ($^3\pi\pi^*$), the Heitler−London approach using the active-electron approximation predicts that the stabilizing exchange interaction is proportional to the overlap density between the singly occupied orbitals (HOMO and LUMO).[39] According to the poor extension of the HOMO in B (i.e., mainly localized on the two oxygen atoms of the terminal carboxylate), we do not expect a large overlap density with the LUMO (i.e., mainly localized on the central pyridine ring, Figure 8), and a poor energy singlet−triplet energy gap should result for B, in contrast with the larger overlap density occurring in A (Figure 7). This prediction is supported by TDDFT calculations which show a significantly larger energy gap for A ($\Delta E_{S-T} = E(^1\pi\pi^*) - E(^3\pi\pi^*) = 0.1785$ eV, Table S7, Supporting Information) than for B ($\Delta E_{S-T} = 0.0216$ eV, Table S8, Supporting Information). Again, this simplified theoretical model qualitatively agrees with the surprisingly small singlet−triplet energy gap observed for [Gd(L13 − 3H)] ($\Delta E_{S-T} = 710$ cm^{-1}) which strongly limits the efficiency of the $^1\pi\pi^* \rightarrow {}^3\pi\pi^*$ intersystem crossing (ISC) process because an optimum minimum gap of 5000 cm^{-1} is required to generate sizable ISC.[40] Consequently, the small ΔE_{S-T} associated with

(38) Hansch, C.; Leo, A.; Taft, R. W. *Chem. Rev.* **1991**, *91*, 165.

(39) (a) Kahn, O. *Adv. Inorg. Chem.* **1995**, *43*, 179. (b) Kahn, O. *Molecular Magnetism*; VCH Publishers: New York, 1993; pp 148−184.

(40) Stemers, F. J.; Verboom, W.; Reinhoudt, D. N.; Vandertol, E. B.; Verhoeven, J. W. *J. Am. Chem. Soc.* **1995**, *117*, 9408.

the introduction of terminal carboxylate groups in [Ln(L13 − 3H)] is a severe handicap for producing efficient metal-centered luminescence (Ln = Eu, Tb) since the efficiency of the ISC process directly affects the sensitization process.[18,41]

Metal-Centered Luminescence. Since the lowest components of the emissive excited *J* manifolds of Eu(III) ($^5D_0$, 17220 cm^{-1})[42] and Tb(III) ($^5D_4$, 20500 cm^{-1})[43] are located, respectively, 6490 and 3210 cm^{-1} below the energy of the ligand-centered $^3\pi\pi^*$ level in [Gd(L13 − 3H)], efficient L13 → Ln(III) (Ln = Eu, Tb) energy transfers are expected. Indeed, irradiation through the ligand levels for [Eu(L13 − 3H)] (**4**) and [Tb(L13 − 3H)] (**6**) provides emission spectra dominated by narrow bands corresponding to the metal-centered $^5D_0 \rightarrow {}^7F_J$ (Ln = Eu, $J = 0-6$, Figure 6c, Table S9, Supporting Information) and $^5D_4 \rightarrow {}^7F_J$ (Ln = Tb, $J = 6-0$, Figure 6d, Table S10, Supporting Information) transitions.[44] However, the broad residual emission of the ligand-centered $^1\pi\pi^*$ excited state observed around 23650 cm^{-1} points to a poor sensitization process and incomplete L13($^1\pi\pi^*$) → Ln(III) energy transfers (Figure 6c,d). Its disappearance in the associated time-resolved spectra (delay time = 0.05 ms) implies that the related L13($^3\pi\pi^*$) → Ln(III) (Ln = Eu, Tb) energy transfer is quantitative, and we can deduce that the $^1\pi\pi^* \rightarrow {}^3\pi\pi^*$ intersystem crossing is the major limiting factor for the metal-centered sensitization in these complexes.

High-resolution emission spectra of [Eu(L13 − 3H)] (**4**) obtained upon excitation through the ligand-centered $^1\pi\pi^*$ state (10−295 K, solid-state) display well-resolved $^5D_0 \rightarrow {}^7F_J$ transitions dominated by the transitions to the $^7F_2$ sublevel (Figures 9 and S4 and Table S9, Supporting Information). At 10 K, the resolution is sufficient for the crystal field splitting to be interpreted in terms of pseudotrigonal symmetry around Eu(III)[33,44] (Table 6) as previously described for $[Eu(L2)_3]^{3+}$ [5a] and $[Eu(L8+H)]^{4+}$ [9] The extremely weak $^5D_0 \rightarrow {}^7F_0$ transition (17209 cm^{-1}, allowed in the C_3 point group)[44] is unique and compatible with one major crystallographic site in the crystal. The two main components of the $^5D_0 \rightarrow {}^7F_1$ transition are assigned to the A (316 cm^{-1}) and E (barycenter = 406 cm^{-1}) sublevels, the latter being split by $\Delta E_{E-E} = 31$ cm^{-1} as a result of distortions from C_3 symmetry.[5a,9,33] The $^5D_0 \rightarrow {}^7F_2$ transition shows two doublets assigned to the electric dipole transitions involving the two E sublevels (E_1 = barycenter 987 cm^{-1}, further split by $\Delta E_{E-E} = 35$ cm^{-1} and E_2 = barycenter 1096 cm^{-1}, further split by $\Delta E_{E-E} = 31$ cm^{-1}, Table 6), and one shoulder ascribed to the A component (1035 cm^{-1}). Finally,

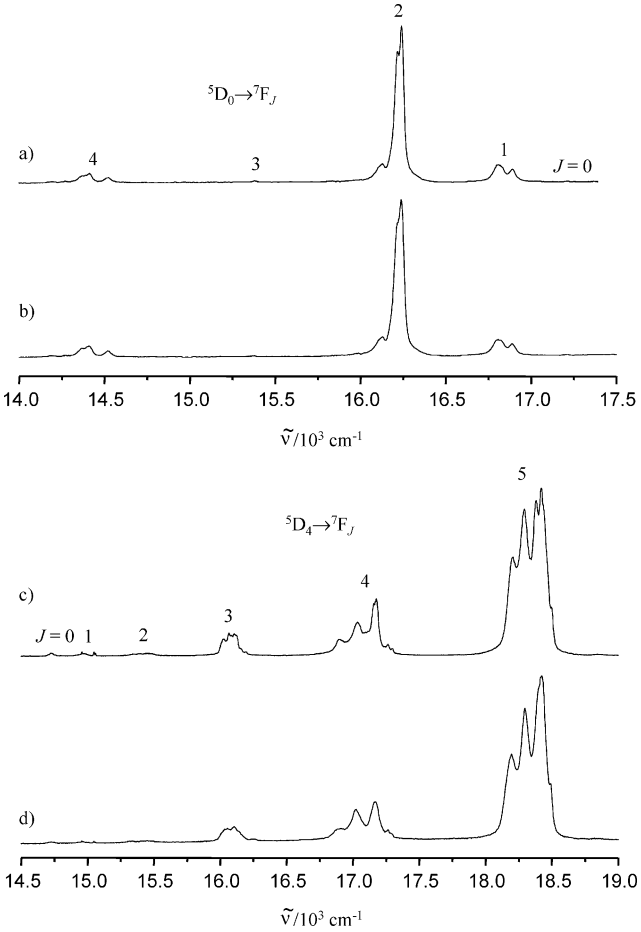

Figure 9. High-resolution emission spetra recorded at 295 K for (a) [Eu(L13 − 3H)] (**4**, solid-state, $\tilde{\nu}_{exc} = 25189$ cm^{-1}), (b) [Eu(L13 − 3H)] (**4**, 10^{-4} M in water, $\nu_{exc} = 25189$ cm^{-1}), (c) [Tb(L13 − 3H)] (**6**, solid-state, $\tilde{\nu}_{exc} = 20491$ cm^{-1}), and (d) [Tb(L13 − 3H)] (**6**, 10^{-4} M in water, $\tilde{\nu}_{exc} = 20491$ cm^{-1}).

Table 6. Energy (cm^{-1}) of the Identified Crystal-Field Sublevels of the Eu(^7F_J) Manifold ($J = 1-4$) in [Eu(L13 − 3H)]·4.4H_2O (**4**) as Determined from Excitation and Emission Spectra in the Solid State at 10 K

$\tilde{\nu}_{ex}$/cm^{-1} site	25252	17205 I	17209 II		25252	17205 I	17209 II
$^7F_0$	0	0	0	$^7F_3$	1833	1825	1824
$^7F_1$	316	317	345	$^7F_4$	2681	2667	2645
	390	383	364		2695	2693	2693
	421	412	397		2791	2798	2803
$^7F_2$	969	966	965		2798	2826	2816
	1004	997	982		2839	2854	2848
	1035	1036	1021		2924	2932	2938
	1080	1070	1080		3019	3014	3016
	1111	1108	1089	$^5D_0$	17209	17205	17209

the $^5D_0 \rightarrow {}^7F_4$ transition shows six components ($3 \times A \rightarrow A$ and $3 \times A \rightarrow E$) in agreement with 3-fold symmetry.[44] This splitting pattern closely matches that reported for [Eu(L8 + H)]$^{4+}$;[9] a careful inspection of the $^5D_0 \rightarrow {}^7F_1$ transition shows that (i) the A level lies at lower energy for both complexes, (ii) the separation between the A and E sublevels increases when going from [Eu(L8 + H)]$^{4+}$ ($\Delta E_{A-E} = 70$ cm^{-1}) to [Eu(L13 − 3H)] ($\Delta E_{A-E} = 90$ cm^{-1}), and (iii) the splitting of the E sublevel concomitantly increases from $\Delta E_{E-E} = 22$ cm^{-1} in [Eu(L8 + H)]$^{4+}$ to $\Delta E_{E-E} = 31$ cm^{-1} in [Eu(L13 − 3H)]. A theoretical approach based on the point charge

(41) (a) Gonçalves e Silva, F. R.; Longo, R.; Malta, O. L.; Piguet, C.; Bünzli, J.-C. G. *Phys. Chem. Chem. Phys.* **2000**, *2*, 5400. (b) Gonçalves e Silva, F. R.; Malta, O. L.; Reinhard, C.; Güdel, H. U.; Piguet, C.; Moser, J. E.; Bünzli, J.-C. G. *J. Phys. Chem. A* **2002**, *106*, 1670 and references therein.
(42) Carnall, W. T.; Fields, P. R.; Rajnak, K. *J. Chem. Phys.* **1968**, *49*, 4450.
(43) Carnall, W. T.; Fields, P. R.; Rajnak, K. *J. Chem. Phys.* **1968**, *49*, 4447.
(44) Bünzli, J,.-C. G. In *Lanthanide Probes in Life, Chemical and Earth Sciences*; Bünzli, J.-C. G., Choppin, G. R., Eds.; Elsevier Publishing Co.: Amsterdam, 1989; Chapter 7.

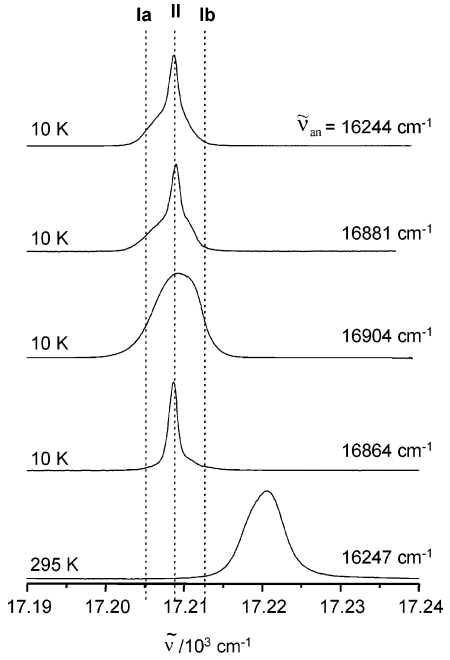

Figure 10. Excitation spectra measured at 10 K and 295 K for [Eu(L13 − 3H)]·4.4H_2O (**4**) in the solid state upon monitoring the Eu($^5D_0 \rightarrow {}^7F_{1,2}$) transitions.

electrostatic model (PCEM) allows an approximate correlation between the splitting of the $^7F_1$ level and the magnitudes and signs of the second-rank crystal-field parameters B_0^2 and B_2^2 in distorted tricapped trigonal prismatic sites.[1b,45] The specific trends noticed under points i−iii provide a semiquantitative analysis of the Ln(III)−ligand interaction in the nine-coordinate podates [Eu(L8 + H)]$^{4+}$ and [Eu(L13 − 3H)]. Point i implies that B_0^2 is negative for both complexes,[1b,45] while points ii and iii indicate that $|B_0^2|$ (proportional to ΔE_{A-E})[1b,45] and $|B_2^2|$ (proportional to ΔE_{E-E})[1b,45] are larger for [Eu(L13 − 3H)] in agreement with a slightly stronger interaction of the ligand with Eu(III) when the terminal carboxamide groups are replaced with negatively charged carboxylates.

The excitation profiles of the Eu($^5D_0 \leftarrow {}^7F_0$) transition in [Eu(L13 − 3H)] obtained upon monitoring the $^5D_0 \rightarrow {}^7F_J$ transitions (J = 1, 2) at 10 K (Figure 10) exhibit two superimposed bands centered at the same energy (17209 cm^{-1}). This is diagnostic for the existence of two different metallic sites I and II, the latter being more rigid (full width at half-height: fwhh = 1.4 cm^{-1}) than the former (fwhh = 6.7 cm^{-1}). Selective irradiation of site I (Ia = 17205 cm^{-1} or Ib = 17213 cm^{-1}, Figure 10) produces an emission spectrum reminiscent of that obtained upon excitation through the ligand-centered excited states and corresponding to the major site in the podate [Eu(L13 − 3H)]. Selective irradiation at 17209 cm^{-1} simultaneously excites both sites I and II and yields a superposition of two emission spectra from which that of site I can be easily recognized and removed (Figure S5, Supporting Information). A detailed analysis of the splitting of the remaining emission spectrum assigned to site II shows only minor differences from that of site I, except for a smaller deviation from C_3 symmetry (Table 6). A population analysis of the $^5D_0 \rightarrow {}^7F_1$ transitions arising from sites I and II upon broad band excitation reveals that site II amounts to only 1% of the total emission, and we conclude that site I (99%) corresponds to the metallic site found in the molecular structure of [Eu(L13 − 3H)]·7H_2O (**8**), while site II (1%) is tentatively assigned to traces of the closely related protonated podate [Eu(L13 − 2H)]$^+$ which is expected to be more rigid and less distorted from C_3 symmetry (the analogous protonated podate [Eu(L8 + H)]$^{4+}$ indeed exhibits crystallographic C_3 symmetry).[9]

Specific donor−Eu(III) interactions can be further compared by measuring the ability of the oxygen atoms of the terminal carboxamide groups ($\delta_{O\text{-amide}}$) in [Eu(L8 + H)]$^{4+}$ and of the carboxylates ($\delta_{O\text{-acid}}$) in [Eu(L13 − 3H)] to produce a nephelauxetic effect according to the Frey and Horrocks equation, eq 8.[46] In this equation, the energy of the Eu($^5D_0 \leftarrow {}^7F_0$) transition ($\tilde{\nu}$) depends on the sum of the nephelauxetic effects produced by the atoms bound to Eu(III) in the first coordination sphere ($\tilde{\nu}_0$ = 17374 cm^{-1} corresponds to the Eu($^5D_0 \leftarrow {}^7F_0$) transition for gaseous Eu(III) at 295 K, and C_{CN} = 1.00 for nine-coordinate Eu-complexes).

$$\tilde{\nu} = \tilde{\nu}_0 + C_{CN} \cdot \sum_i n_i \cdot \delta_i \qquad (8)$$

Taking $\delta_{N-pyridine}$ = −15.3 previously determined for bound heterocyclic nitrogen atoms[5a,47] and introducing $\tilde{\nu}$ = 17225 cm^{-1} for [Eu(L8 + H)]$^{4+}$ [9] and $\tilde{\nu}$ = 17220 cm^{-1} for [Eu(L13 − 3H)] at 295 K (Figure 10), one equation is obtained for each podate (17225 = 17374 + 3$\delta_{N\text{-pyridine}}$ + 6$\delta_{O\text{-amide}}$ and 17220 = 17374 + 3$\delta_{N\text{-pyridine}}$ + 3$\delta_{O\text{-amide}}$ + 3$\delta_{O\text{-acid}}$) from which $\delta_{O\text{-amide}}$ = −17.2 and $\delta_{O\text{-acid}}$ = −18.8 can be calculated. These values are in line with $\delta_{O\text{-amide}}$ = −15.7 and $\delta_{O\text{-acid}}$ = −17.2 extracted by multilinear least-squares fits of a large collection of nine-coordinate Eu(III) complexes[46] and point to a slightly larger charge delocalization onto the carboxylate group which results from a stronger interaction with Eu(III).[46,48] This observation confirms the marginally shorter Ln−O(carboxylate) bond distances found in **8** and the trend established for the second-rank crystal-field parameters which eventually demonstrates that the carboxylate groups display slightly stronger interactions with Ln(III) than carboxamides. Finally, the Eu($^5D_0$) and Tb($^5D_4$) lifetimes of [Ln(L13 − 3H)] (Ln = Eu, Tb) in the solid state are similar to those reported for the related deprotonated podates [Ln(L8)]$^{3+}$ (Table S11, Supporting Information).[9] This points to (i) inefficient Tb $\rightarrow {}^3\pi\pi^*$ energy back-transfer processes and (ii) no water molecule bound to Eu(III) or Tb(III)[36] as supported by the molecular structures of [Ln(L13 − 3H)]·7H_2O (Ln = Eu, **8**; Tb, **9**).

Solution Structure and Quantum Yields of [Ln(L13−3H)]·xH_2O (Ln = Eu, x = 4.4, 4; Tb, x = 7.3,

(45) Binnemans, K.; Görller-Walrand, C. *Chem. Phys. Lett.* **1995**, *245*, 75.
(46) Frey, S. T.; Horrocks, W. DeW., Jr. *Inorg. Chim. Acta* **1995**, *229*, 383.
(47) Petoud, S.; Bünzli, J.-C. G.; Schenk, K. J.; Piguet, C. *Inorg. Chem.* **1997**, *36*, 1345.
(48) Albin, M.; Horrocks, W. DeW., Jr. *Inorg. Chem.* **1985**, *24*, 895.

6). Since the podates [Ln(L13 − 3H)] are only poorly soluble in water at pH = 8 ($\leq 10^{-4}$ M), NMR spectra cannot be easily recorded, and we have resorted to high-resolution spectroscopy for investigating the solution structure of [Eu(L13 − 3H)] and [Tb(L13 − 3H)]. The absorption, excitation, and emission spectra obtained in solution (water, 10^{-4} M, pH = 8) are almost identical to those recorded in the solid state (Figure 9, Tables S9 and S10, Supporting Information), which demonstrates that the nine-coordinate pseudotricapped trigonal prismatic geometry is maintained in solution. According to the formation constants $\log(\beta_{110}^{Ln}) = 6.7(2)$ found for [Gd(L13 − 3H)] (eq 7, Table 1), we calculate that [Ln(L13 − 3H)] (Ln = Eu, Tb) accounts for more than 92% of the ligand speciation, and the monoexponential lifetimes measured for the Eu($^5D_0$) and Tb($^5D_4$) levels in solution reflect nine-coordinate environments similar to those found in the solid state. Interestingly, τ(Eu($^5D_0$)) and τ(Tb($^5D_4$)) for [Ln(L13 − 3H)] in water are marginally shorter than those measured in the solid state, but those recorded in D_2O in the same conditions are slightly longer (Tables S11 and S12, Supporting Information). This suggests that some interactions occur in solution between the high-frequency OH oscillators and the metallic center. The use of the Horrocks and Sudnick[49] equation, eq 9, corrected for closely diffusing OH oscillators[36] gives $q = 0.1-0.2$ for [Eu(L13 − 3H)] and $q = 0.3-0.5$ for [Tb(L13 − 3H)] (Table S12, Supportin Information; q is the number of water molecules in the first coordination sphere (±0.3), k_{H_2O} and k_{D_2O} are the decay rate constants (ms^{-1}) for [Ln(L13 − 3H)] in H_2O and D_2O, respectively, Δk_{corr} is a correcting factor for closely diffusing OH oscillators: $\Delta k_{corr}^{Eu} = 0.25$ ms^{-1}, $\Delta k_{corr}^{Tb} = 0.06$ ms^{-1}, and $A_{Eu} = 1.2$ ms and $A_{Tb} = 5$ ms).[36,49] This confirms the absence of water molecule in the first coordination sphere of the Ln(III) ion, but some weak second sphere interactions affect the luminescence of the Tb-containing podate.

$$q = A(k_{H_2O} - k_{D_2O} - \Delta k_{corr}) \tag{9}$$

Although the absolute quantum yields measured in pure water at pH = 8 remain modest $\Phi_{tot}^{Eu} = 1.8 \times 10^{-3}$ and $\Phi_{tot}^{Tb} = 8.9 \times 10^{-3}$, they are significantly larger than those reported for $[Ln(L8)]^{3+}$ in a 4:1 acetonitrile/water mixture ($\Phi_{tot}^{Eu} = 2.4 \times 10^{-5}$ and $\Phi_{tot}^{Tb} = 2.9 \times 10^{-3}$).[9] At first sight, the increase of Φ_{tot}^{Eu} by 2 orders of magnitude in [Eu(L13 − 3H)] could be assigned to the rigidification of the coordination sphere by the carboxylate groups bound to Eu(III) ($q = 0$ for both podates $[Eu(L8)]^{3+}$ and in [Eu(L13 − 3H)]).[9] However, this feature mainly influences the final lanthanide luminescence step Φ^{Eu}, but the overall antenna effect involves a multistep mechanism[3,18,40,41] in which (i) UV light is first collected by the singlet ligand-centered states, and then (ii) $^1\pi\pi^* \rightarrow {}^3\pi\pi^*$ conversion occurs (η_{ISC}) followed by (iii) energy transfer from the ligand-centered to the metal-centered excited states ($^3\pi\pi^* \rightarrow$ Ln, η_{ET}), and (iv) metal-centered visible light emission (Ln = Eu, Tb, Φ^{Ln}). The total quantum yield Φ_{tot}^{Eu} is thus given by eq 10,[3a,36,50] and the replacement of the terminal carboxamides in $[Eu(L8)]^{3+}$ with carboxylates in [Eu(L13 − 3H)] may affect any step.

$$\Phi_{tot}^{Eu} = \eta_{ISC}\eta_{ET}\Phi^{Eu} = \eta_{sens}\Phi^{Eu} \tag{10}$$

We have thus determined the quantum yield Φ^{Eu} of the lanthanide luminescence step in order to better understand the origin of the beneficial "carboxylate effect" observed in [Eu(L13 − 3H)]. If we assume that the dipole strength of the magnetic dipole Eu($^5D_0 \rightarrow {}^7F_1$) transition is constant (a reasonable assumption),[1b,44] the radiative lifetime τ_R of the Eu($^5D_0$) level is given by eq 11 in which $A_{MD,0} = 14.65$ s^{-1} is the spontaneous emission probability of the Eu($^5D_0 \rightarrow {}^7F_1$) transition, n is the refractive index of the solvent ($n = 1.334$ for water), and I_{MD}/I_{tot} is the ratio of the area of the Eu($^5D_0 \rightarrow {}^7F_1$) transition to the area of the $^5D_0 \rightarrow {}^7F_J$ transitions ($J = 0-6$) of [Eu(L13 − 3H)].[50]

$$\tau_R = \frac{1}{A_{MD,0}n^3}\left(\frac{I_{MD}}{I_{tot}}\right) \tag{11}$$

We experimentally observe $I_{MD}/I_{tot} = 0.143$ and calculate $\tau_R = 4.1$ ms, which is in good agreement with $\tau_R = 4.3$ ms previously reported for the analogous trigonal complex $[Eu(L1 - 2H)_3]^{3-}$ in water.[50] We can then deduce that $\Phi^{Eu} = \tau_{obs}/\tau_R = 0.28$ for [Eu(L13 − 3H)] and $\Phi^{Eu} = 0.31$ for $[Eu(L1 - 2H)_3]^{3-}$ [51] in agreement with a rather efficient metal-centered emission and a satisfying structural and electronic optimization of the metallic coordination sphere. Since the total quantum yield Φ_{tot}^{Eu} is given by eq 10, the limited quantum yield found for [Eu(L13 − 3H)] is assigned to an inefficient sensitization process ($\eta_{sens} = 6.4 \times 10^{-3}$) which can be compared with $\eta_{sens} = 6.1 \times 10^{-2}$ calculated for $[Eu(L1 - 2H)_3]^{3-}$.[16] Similar calculations using the data reported for the Eu-podates with L8 in acetonitrile[9] give $\tau_R = 3.5$ ms, $\Phi^{Eu} = 0.55$, and $\eta_{sens} = 2.7 \times 10^{-4}$ for $[Eu(L8 + H)]^{4+}$, and $\tau_R = 3.3$ ms, $\Phi^{Eu} = 0.50$, and $\eta_{sens} = 2.2 \times 10^{-4}$ for $[Eu(L8)]^{3+}$. The lower quantum yield of the europium luminescence step observed when carboxamides in $[Eu(L8)]^{3+}$ are replaced with carboxylates in [Eu(L13 − 3H)] suggests some de-excitation of the Eu($^5D_0$) level induced by second-sphere water molecules interacting with the noncoordinated oxygen atoms of the carboxylate groups, as found in the crystal structure of **8**. However, the change in Φ^{Eu} between $[Eu(L8)]^{3+}$ and [Eu(L13 − 3H)] accounts only for a factor of 2 which is negligible compared with the 100-fold increase of the total quantum yield in [Eu(L13 − 3H)]. We conclude that the beneficial carboxylate effect detected in [Eu(L13 − 3H)] indeed results from a slightly improved sensitization process. Separation of η_{ISC} and η_{ET} is not accessible without a sophisticated theoretical modeling[41] or

(49) (a) Horrocks, W. DeW., Jr.; Sudnick, D. R. *J. Am. Chem. Soc.* **1979**, *101*, 334. (b) Horrocks, W. DeW., Jr.; Sudnick, D. R. *Science* **1979**, *206*, 1194. (c) Horrocks, W. DeW., Jr.; Sudnick, D. R. *Acc. Chem. Res.* **1981**, *14*, 384.

(50) Werts, M. H. V.; Jukes, R. T. F.; Verhoeven, J. W. *Phys. Chem. Chem. Phys.* **2002**, *4*, 1542.

(51) The Eu($^5D_0$) lifetime of $[Eu(L1 - 2H)_3]^{3-}$ has been taken from ref 16 and from: Lis, S.; Choppin, G. *J. Alloys Compd.* **1995**, *225*, 257.

a quantitative analysis of the ligand-centered emission properties,[52] but it is worth noting that previous detailed investigations of the sensitization process in the closely related complex $[Eu(L5)_3]^{3+}$ concluded that η_{ISC} was the major limiting factor of the antenna effect.[41a,52]

Conclusion

Our detailed investigations of the nine-coordinate lanthanide-containing podates derived from L8 and L13 eventually provide a balance of advantages and drawbacks due to the replacement of terminal carboxamide groups with carboxylates.

Synthetic Aspects. The introduction of two different sidearms at the 2 and 6 positions of the pyridine ring in L13 complicates the synthetic strategy, and the introduction of specific protecting groups compatible with the final selective hydrolysis limits the synthetic access to these receptors. Moreover, the carboxylic acids are generally involved in self-complementary H-bonding networks[30,53] which require the use of strongly competing (i.e., polar) solvents for producing significant solubility (L13 is only reasonably soluble in water). Finally, the apical nitrogen atom of the Me−TREN tripod is significantly more basic in $[L13 - 3H]^{3-}$ than in L8 (2 orders of magnitude). The formation of the deprotonated podate $[L13 - 3H]^{3-}$ thus requires basic conditions, a drawback for the complexation of Ln(III) ions which are partially hydrolyzed for pH $\geq$ 8.0.

Thermodynamic and Structural Aspects. The considerable affinity of the negatively charged carboxylate groups for the oxophilic Ln(III) overcomes competition with water, and stable neutral podates [Ln(L13 − 3H)] can be obtained in pure water, while $[Ln(L8)]^{3+}$ species are quantitatively decomplexed when 20% water is added into acetonitrile.[9] However, the molecular structures of [Eu(L13 − 3H)] and $[Eu(L8 + H)]^{4+}$ are very similar (Figure S3), and the Eu−O(carboxylate) bonds are only marginally shorter than the Eu−O(carboxamide) bonds which points to similar enthalpic contents in the two podates. This suggests that the impressive stabilization of [Ln(L13 − 3H)] in water, and more generally of lanthanide complexes with carboxylato-containing ligands, has an entropic origin due to (i) the charge compensation occurring when $[L13 - 3H]^{3-}$ reacts with Ln^{3+},[14] and (ii) the increase of the translational entropy produced upon desolvation of the charged receptors.[3,4,54] However, the small residual charge borne by the final polar complexes drastically limits solubility in polar and nonpolar solvents, and the neutral podates [Ln(L13 − 3H)] are only sparingly soluble in water ($\leq 10^{-4}$ M), a severe drawback for the design of functional molecular devices and sensors.

Electronic Aspects. Our theoretical TDDFT calculations suggest that the negative charge and the poor electron-withdrawing capacity of the carboxylate groups connected at the 6-position of the pyridine in L13 have two main consequences on the ligand-centered excited states. (1) The HOMO−LUMO gap is reduced when a terminal carboxamide is replaced with a carboxylate, which translates into a 2000 cm^{-1} red-shift of $^1\pi\pi^*$ when going from $[Gd(L8 + H)]^{4+}$ to [Gd(L13 − 3H)]. (2) The lowest $^1\pi\pi^*$ and $^3\pi\pi^*$ levels possess a considerable carboxylate → pyridine charge-transfer character which strongly limits the contribution of the exchange interaction to the stabilization of the $^3\pi\pi^*$ level. Consequently, the energies of the ligand-centered $^1\pi\pi^*$ and $^3\pi\pi^*$ levels are close (ΔE_{S-T} = 710 cm^{-1} for [Gd(L13 − 3H)]) which affects the efficiency of the $^1\pi\pi^* \rightarrow {}^3\pi\pi^*$ intersystem crossing (ISC) process,[40] and of the overall antenna effects in the luminescent complexes [Ln(L13 − 3H)] (Ln = Eu, Tb).

We thus conclude that the replacement of terminal carboxamides in $[Ln(L8)]^{3+}$ with carboxylates in [Ln(L13 − 3H)] provides advantages (stability in water, rigidity of the coordination sphere, large lanthanide quantum yields) which are balanced by severe drawbacks (low solubility and limited sensitization), a situation remote from the Eldorado suggested by the large stability and quantum yield observed for $[Eu(L12 - 2H)]^+$ (Φ_{Eu}^{tot} = 0.12)[13] and $[Eu(L')]^-$ (Φ_{Eu}^{tot} = 0.16, L′ is a multidentate ligand bearing two terminal iminodacetic units bound to a central tridentate anchor).[55] Since Φ^{Eu} = 0.28 in [Eu(L13 − 3H)] (and q = 0), further improvements of the structural and electronic control of the lanthanide coordination sphere may lead to a maximum gain of a factor 4 in the total quantum yield ($\Phi_{tot,maximum}^{Eu} \approx 4 \times 1.8 \times 10^{-3} = 7.2 \times 10^{-3}$). This remains desperately low compared with Φ_{Eu}^{tot} = 0.12 reported for $[Eu(L12 - 2H)]^+$ in water,[13] and we suspect that specific electronic effects resulting from the synergistic connection of one carboxylate and one pyridine substituent at the 2 and 6 positions of the central pyridine ring in L12 are responsible for the remarkable increase of the efficiency of the sensitization process ($\eta_{sens} > 0.1$) in the final lanthanide podates $[Ln(L12 - 2H)]^+$ as previously evidenced in $[Ln(L')]^-$ (η_{sens} = 0.1−1.0).[55] Nevertheless, the connection of terminal carboxylates remains attractive for the preparation of water-stable and structurally controlled nine-coordinate lanthanide sites in polymetallic podates and helicates.[3,15] Moreover, our detailed luminescence study demonstrates that the replacement of the terminal carboxamide groups with carboxylates increases the second-rank crystal-field and nephelauxetic parameters, a crucial point for manipulating magnetic anisotropy (i.e., orientation in magnetic field)[2,56] and spin delocalization (i.e., outer sphere relaxation in MRI contrast agents)[57] in molecular complexes or mesomorphic materials.

(52) Petoud, S.; Bünzli, J.-C. G.; Piguet, C.; Xiang, Q.; Thummel, R. *J. Lumin.* **1999**, *82*, 69.
(53) Braga, D. *J. Chem. Soc., Dalton Trans.* **2000**, 3705.
(54) (a) Caravan, P.; Hedlund, T.; Liu, S.; Sjöberg, S.; Orvig, C. *J. Am. Chem. Soc.* **1995**, *117*, 11230. (b) Lowe, M. P.; Caravan, P.; Rettig, S. J.; Orvig, C. *Inorg. Chem.* **1998**, *37*, 1637.
(55) Brunet, E.; Juanes, O.; Sedano, R.; Rodriguez-Ubis, J.-C. *Photochem. Photobiol. Sci.* **2002**, *1*, 613.
(56) Mironov, V. S.; Galyametdinov, Y. G.; Ceulemans, A.; Binnemans, K. *J. Chem. Phys.* **2000**, *113*, 10293.
(57) (a) Aime, S.; Botta, M.; Fasano, M.; Terreno, E. *Chem. Soc. Rev.* **1998**, *27*, 19. (b) Aime, S.; Botta, M.; Dickins, R. S.; Maupin, C. L.; Parker, D. A.; Riehl, J. P.; Williams, J. A. G. *J. Chem. Soc., Dalton Trans.* **1998**, 881. (c) Caravan, P.; Ellison, J. J.; McMurry, T. J.; Lauffer, R. B. *Chem. Rev.* **1999**, *99*, 2293.

Table 7. Summary of Crystal Data, Intensity Measurements, and Structure Refinement for [Ln(L13 − 3H)]·7H_2O (Ln = Eu, **8**; Ln = Tb, **9**, Ln = Lu, **10**)

	8	**9**	**10**
formula	$EuC_{30}H_{44}N_7O_{16}$	$TbC_{30}H_{44}N_7O_{16}$	$LuC_{30}H_{44}N_7O_{16}$
mol wt	910.8	917.7	933.8
color	colorless	colorless	colorless
cryst syst	monoclinic	monoclinic	monoclinic
space group	$P2_1/c$	$P2_1/c$	$P2_1/c$
a, Å	18.2939(13)	18.2552(14)	18.0922(9)
b, Å	15.3296(7)	15.3040(8)	15.2671(9)
c, Å	13.0475(9)	13.0819(9)	13.0475(7)
β, deg	92.862(9)	92.580(9)	92.738(6)
V, Å^3	3654.5(4)	3651.1(4)	3599.8(3)
Z	4	4	4
d_{calcd}, g·cm^{-3}	1.655	1.669	1.723
μ(Mo Kα), mm^{-1}	1.80	2.02	2.83
T_{min}/T_{max}	0.7112/0.8793	0.6782/0.7937	0.6537/0.7423
cryst size, mm^3	0.072 × 0.175 × 0.225	0.12 × 0.19 × 0.19	0.115 × 0.152 × 0.165
2θ range	5.7° < 2θ < 56.1°	5.4° < 2θ < 55.9°	5.7° < 2θ < 56.0°
reflns measured	39090	38784	38573
reflns unique	8485	8757	8704
R_{int}	0.049	0.049	0.053
obsd ($\|F_o\| > 4\sigma(F_o)$)	5341	5629	5259
max and min $\Delta\rho$, e Å^{-3}	0.92/−1.40	1.00/−0.67	1.41/−3.26
weighting scheme w	$1/(\sigma^2(F_o) + 0.0001(F_o)^2)$	$1/(\sigma^2(F_o) + 0.0002(F_o)^2)$	$1/(\sigma^2(F_o) + 0.0001(F_o)^2)$
GOF[a]	1.24(1)	1.03(1)	1.23(1)
R,[b] R_w[c]	0.026/0.025	0.022/0.022	0.030/0.027

[a] GOF = $[\sum\{((F_o - F_c)/\sigma(F_o))^2\}/(N_{ref} - N_{var})]^{1/2}$. [b] $R = \sum||F_o| - |F_c||/\sum|F_o|$. [c] $R_w = [\sum(w|F_o| - |F_c|)^2/\sum w|F_o|^2\ ]^{1/2}$.

Experimental Section

Solvents and Starting Materials. These were purchased from Fluka AG (Buchs, Switzerland) and used without further purification unless otherwise stated. Thionyl chloride was distilled over elemental sulfur, acetonitrile, dichloromethane, *N*,*N*-dimethylformamide, and triethylamine over CaH_2, and pyridine over Na. Silica gel (Acros, 0.035−0.07 mm) was used for preparative column chromatography. Tris(2-(*N*-methylamino)ethyl)amine (**2**)[19] and 2-carboxy-6-methylpyridine[58] were prepared according to literature procedures. The perchlorate salts Ln$(ClO_4)_3.xH_2O$ (Ln = La−Lu, x = 6−8) were prepared from the corresponding oxides (Rhodia, 99.99%) and dried according to published procedures.[59] The Ln content of solid salts was determined by complexometric titrations with Titriplex III (Merck) in the presence of urotropine and xylene orange.[60] The syntheses and characterizations of the ligand tris{2-[*N*-methylcarbamoyl-(6-carboxypyridine-2)ethyl]amine} (L13) and its complexes [Ln(L13 − 3H)]·xH_2O (Ln = Eu, x = 4.4, **4**; Gd, x = 6.5, **5**; Tb, x = 7.3, **6**; Lu, x = 3.8, **7**) are given in the Supporting Information.

Caution. Dry perchlorates may explode and should be handled in small quantities and with the necessary precautions.[61]

Crystal-Structure Determination of Ln[(L13 − 3H)]·7H_2O (Ln = Eu, Tb, Lu). The complexes Ln[(L13 − 3H)]·7H_2O (Ln = Eu, **8**; Tb, **9**; Lu, **10**) were isostructural. A summary of the crystal data, intensity measurements, and structure refinements is reported in Table 7. Cell dimensions and intensities were measured at 200 K on a Stoe IPDS diffractometer with graphite-monochromated Mo Kα radiation (λ = 0.7107 Å). The structures were solved by direct methods (SIR97)[62] and refined by full-matrix least-squares based on F. All other calculations were performed with XTAL[63] system and ORTEP[64] programs. The water molecule O7w was disordered and refined on two atomic sites with population parameters PP = 0.8/0.2 for complexes **8** and **9**, and PP = 0.6/0.4 for **10**. All non-H atoms (except the minor site of O7w) were refined with anisotropic displacement parameters. The hydrogen atoms of the water molecules and of the methyl groups were refined with restraints on bond distances and bond angles and blocked during the last cycles for **10**. All other hydrogen atoms were observed and refined with a fixed displacement parameter. CCDC-205045, CCDC-205046, and CCDC-205047 contain the supplementary crystallographic data for Ln[(L13 − 3H)]·7H_2O (Ln = Eu, **8**; Ln = Tb, **9** and Ln = Lu, **10**, respectively). These data can be obtained free of charge via www.ccdc.cam.ac.uk/conts/retrieving.html. (Data are also available from the Cambridge Crystallographic Data Centre, 12 Union Road, Cambridge CB2 1EZ, U.K. Fax: (+ 44) 1223-336-033. E-mail: deposit@ccdc.cam.ac.uk.)

Spectroscopic and Analytical Measurements: Reflectance spectra were recorded as finely ground powders dispersed in MgO (5%) with MgO as reference on a Perkin-Elmer Lambda 900 spectrophotometer equipped with a PELA-1020 integrating sphere from Labsphere. Electronic absorption spectra in the UV−vis were recorded at 25 °C from solutions in water with a Perkin-Elmer Lambda 900 spectrometer using quartz cells of 0.1 and 1 mm path length. Spectrophotometric titrations were performed with a J&M diode array spectrometer (Tidas series) connected to an external computer. In a typical experiment, 50 mL of L13·3H_2O in water (10^{-4} M + 0.05 M tris(hydroxymethyl)aminomethane−HCl, pH = 8) was titrated at 25 °C with a solution of Ln$(ClO_4)_3$·nH_2O (10^{-3} M) in water under an N_2 atmosphere. After each addition of 0.10 mL, the absorbances were recorded using a Hellma optrode (optical path length 0.5 cm) immersed in the thermostated titration vessel and connected to the spectrometer. Mathematical treatment of the

(58) Black, G.; Depp, E.; Corson, B. B. *J. Org. Chem.* **1949**, *14*, 14−21.
(59) Desreux, J.-F. In *Lanthanide Probes in Life, Chemical and Earth Sciences*; Bünzli, J.-C. G., Choppin, G. R., Eds.; Elsevier Publishing Co.: Amsterdam, 1989; Chapter 2, p 43.
(60) Schwarzenbach, G. *Complexometric Titrations*; Chapman & Hall: London, 1957 p 8.
(61) Wolsey, W. C. *J. Chem. Educ.* **1978**, *50*, A335.
(62) Altomare, A.; Burla, M. C.; Camalli, M.; Cascarano, C. G.; Giacovazzo, C.; Guagliardi, A.; Moliterni, A. G. G.; Polidori, G.; Spagna, R. *J. Appl. Crystallogr.* **1999**, *32*, 115.
(63) *XTAL 3.2 User's Manual*; Hall, S. R., Flack, H. D. M., Stewart, J. M., Eds.; Universities of Western Australia and Maryland, 1989.
(64) Johnson, C. K. *ORTEP II.*; Report ORNL-5138; Oak Ridge National Laboratory: Oak Ridge, TN, 1976.

spectrophotometric titrations was performed with factor analysis[28] and with the SPECFIT program.[29] Potentiometric titrations were performed under an inert atmosphere in a thermostated titration vessel (25 °C) equipped with a pH electrode Metrohm 6.0202.000 connected to a pH meter Metrohm 691. In a typical experiment, 50 mL of ligand L13·3H_2O (10^{-3} M) in water/acetonitrile (95:5) containing $NaClO_4$ (0.1 M) was titrated with a solution of sodium hydroxide 0.05 M in the same solvent. After each addition of 0.05 mL, the pH was recorded and transferred to a computer. After the addition of 4 equivs of NaOH, the solution was titrated with hydrochloric acid 0.05 M by using the same experimental setup. A model for the distribution of species was fitted with a nonlinear least-squares algorithm to give acid−base constants. IR spectra were obtained from KBr pellets with a Perkin-Elmer 883 spectrometer. ^{1}H NMR spectra were recorded at 25 °C on a Broadband Varian Gemini 300 spectrometer. Chemical shifts are given in ppm versus TMS. EI-MS (70 eV) were recorded with VG-7000E and Finnigan-4000 instruments. Pneumatically assisted electrospray (ESI-MS) mass spectra were recorded from 10^{-4} M solutions on API III and API 3000 tandem mass spectrometers (AB/MDS Sciex). The experimental procedures for high-resolution, laser-excited luminescence measurements have been published previously.[65] Solid-state samples were finely powdered, and the low temperature (295−10 K) was achieved by means of a Cryodyne Model 22 closed-cycle refrigerator from CTI Cryogenics. Luminescence spectra were corrected for the instrumental function, but not excitation spectra. Lifetimes are averages of at least 3−5 independent determinations and were measured using excitation provided by a Quantum Brillant Nd:YAG laser equipped with frequency doubler, tripler, and quadrupler as well as with an OPOTEK MagicPrism OPO crystal. Ligand excitation and emission spectra, as well as quantum yields, were recorded on a Perkin-Elmer LS-50B spectrometer equipped for low-temperature measurements. The quantum yields Φ have been calculated using the equation $\Phi_x/\Phi_r = (A_r(\tilde{\nu})I_r(\tilde{\nu})n_x^2D_x)/(A_x(\tilde{\nu})\cdot I_x(\tilde{\nu})n_r^2D_r)$, where x refers to the sample and r to the reference; A is the absorbance, $\tilde{\nu}$ the excitation wavenumber used, I the intensity of the excitation light at this energy, n the refractive index, and D the integrated emitted intensity. $[Eu(terpy)_3](ClO_4)_3$ (Φ = 1.3%, acetonitrile, 10^{-3} M) and $[Tb(terpy)_3](ClO_4)_3$ (Φ = 4.7%, acetonitrile, 10^{-3} M) were used as references for the determination of quantum yields of respectively Eu- and Tb-containing samples.[5a,52] Elemental analyses were performed by Dr. H. Eder from the microchemical Laboratory of the University of Geneva.

Computational Details. TDDFT calculations have been restricted to a single tridentate binding unit corresponding to one ligand strand taken from the crystal structures of $[Eu(L8 + H)](CF_3SO_3)_3(PF_6)(CH_3CN)_{0.5}$[9] (binding unit A) and [Eu(L13−3H)]·7H_2O (**8**, binding unit B). The ethyl groups of the terminal carboxamides are replaced by methyl groups to limit extensive calculations in A. Calculations of singlet−singlet and singlet−triplet excitation energies have been performed using the Amsterdam Density Functional program (ADF 2002.02).[66] A Slater-type orbitals TZ2P basis set (double-ζ in core, triple-ζ in the valence region + 2 polarization functions) has been used for the C, O, N, and H atoms. To ensure a correct asymptotic behavior to the exchange-correlation potential, the statistical average of orbital potential (SAOP)[67] has been chosen for the TDDFT calculations. All the calculations have been performed on a Silicon Graphics O2 workstation and on a cluster of PCs.

Acknowledgment. We are grateful to Ms. Hélène Lartigue, Mr. Laurent Gaudard, and Mr. Frédéric Gumy for technical assistance. This work is supported through grants from the Swiss National Science Foundation.

Supporting Information Available: Additional synthetic details, figures, and tables. Crystal data in CIF files for **8**, **9**, and **10**. This material is available free of charge via the Internet at http://pubs.acs.org.

IC034231T

(65) Rodriguez-Cortinas, R.; Avecilla, F.; Platas-Iglesias, C.; Imbert, D.; Bünzli, J.-C. G.; de Blas, A.; Rodriguez-Blas, T. *Inorg. Chem.* **2002**, *41*, 5336.

(66) Te Velde, G.; Bickelhaupt, F. M.; Baerends, E. J.; Fonseca Guerra, C.; van Gisbergen, S. J. A.; Snijders, J. G.; Ziegler T. J. *Comput. Chem.* **2001**, *22*, 931.

(67) Schipper, P. R. T.; Gritsenko, O. V.; van Gisbergen, S. J. A.; Baerends, E. J. *J. Chem. Phys.* **2000**, *112*, 1344.